

NASA/TM—1998-208659



14-57
452-207

Space Shuttle Pinhole Formation Mechanism Studies

Nathan S. Jacobson
Lewis Research Center, Cleveland, Ohio

National Aeronautics and
Space Administration

Lewis Research Center

November 1998

Acknowledgments

It is a pleasure to acknowledge the many individuals who assisted with the exposure and analyses of these specimens. We thank Donald Humphrey of NYMA/NASA Lewis Group for the furnace exposure of the RCC and SiC materials. For specimen preparation, we thank Todd Leonhardt, formerly of NYMA/NASA Lewis. For the SEM study, we thank Pat Dickerson, formerly of NYMA/NASA Lewis Group, David Hull of NASA Lewis, and Terry McCue of NYMA/NASA Lewis Group. For the EPMA study, we thank Bill Blackburn of Binghamton University, Binghamton, NY. The support and guidance of Dr. Donald Curry, NASA-JSC, is very much appreciated.

Trade names or manufacturers' names are used in this report for identification only. This usage does not constitute an official endorsement, either expressed or implied, by the National Aeronautics and Space Administration.

Available from

NASA Center for Aerospace Information
7121 Standard Drive
Hanover, MD 21076
Price Code: A00

National Technical Information Service
5285 Port Royal Road
Springfield, VA 22100
Price Code: A00

SPACE SHUTTLE PINHOLE FORMATION MECHANISM STUDIES

Nathan S. Jacobson
National Aeronautics and Space Administration
Lewis Research Center
Cleveland, Ohio 44135

SUMMARY

Pinholes have been observed to form on the wing leading edge of the space shuttle after about 10 to 15 flights. In this report we expand upon previous observations by Christensen (ref. 1) that these pinholes often form along cracks and are associated with a locally zinc-rich area. The zinc appears to come from weathering and peeling paint on the launch structure. Three types of experimental examinations are performed to understand this issue further: (a) Detailed microstructural examination of actual shuttle pinholes (b) Mass spectrometric studies of coupons containing actual shuttle pinholes and (c) Laboratory furnace studies of ZnO/SiC reactions and ZnO/SiC protected carbon/carbon reaction. On basis on these observations we present a detailed mechanism of pinhole formation due to formation of a corrosive ZnO-Na₂O-SiO₂ ternary glass, which flows into existing cracks and enlarges them.

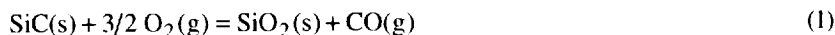
INTRODUCTION

Material Description

The wing leading edge and nose cap of the space shuttle orbiter is composed of a reinforced carbon/carbon (RCC) material. The location of these panels on the orbiter is shown in figure 1. A diagram of the RCC material is shown schematically in figure 2 and described in more detail in reference 1. It consists of layers of a graphitized rayon fabric, which are repeatedly impregnated with a liquid carbon precursor. Pyrolysis then converts the precursor to carbon. A diffusion conversion coating of silicon carbide is then grown on the surface at high temperatures by a pack siliconizing cementation technique. Next the material is vacuum infiltrated with tetraethyl orthosilicate (TEOS) to fill cracks and fissures. On heating, the TEOS decomposes to silica. The outer layer is a proprietary sealant of 'Type A' glass, which is primarily sodium silicate. This is intended to flow into the cracks which develop in the SiC.

An important issue with this system is the thermal expansion mismatch between the SiC coating and the carbon/carbon. Cracks develop in the SiC coating during processing and also during service. Figure 3 and the associated oxygen map illustrate these two types of cracks. The crack which developed during processing is filled with pure silica, as indicated by the oxygen map. No other elements were detected in this crack. The crack which developed during testing is visible in the image as an open crack.

At this point it is appropriate to discuss the oxidation of SiC and the effect of a sodium silicate glass coating. Oxidation of SiC has been extensively studied and recently reviewed in detail (ref. 2). The process is illustrated in figure 4(a). Oxygen permeates a growing SiO₂ film and reacts with SiC at the SiC/SiO₂ interface, according to:



The rate controlling step is the permeation of oxygen inward through the SiO₂ network. As the reaction proceeds CO(g) must escape from the reaction interface, either by a permeation process through the SiO₂ scale or, in some cases, by forming bubbles in the SiO₂. Generally bubbles in SiO₂ indicate a large amount gas escaping and hence a vigorous reaction.

Small amounts of foreign cations, such as Na or K, tend to act as network modifiers, breaking up the SiO₂ network and allowing faster oxygen transport and hence faster oxidation rates (ref. 2). Controlled studies of cation modified SiO₂ scales indicate that these cations can accelerate oxidation rates by up to 10X (ref. 2). Larger amounts of cations, as added oxides (e.g., Na₂O) may react with the SiO₂ to form low melting eutectic liquids which have rapid transport rates and allow for rapid oxidation. Figure 5 is the Na₂O-SiO₂ binary phase diagram (ref. 3). It follows that when a Na₂O.x(SiO₂) liquid is applied to a SiO₂-forming ceramic, the equilibrium situation is illustrated in figure 4(b). The composition of the liquid silicate at the silicate/SiO₂ interface is given by the liquidus

(liquid/tridymite + liquid line) in figure 5 (refs. 2 and 4). In this case with the RCC material, when $\text{Na}_2\text{O} \cdot x(\text{SiO}_2)$ is added to the a pre-existing SiO_2 film on SiC, one would expect the SiO_2 to dissolve in the $\text{Na}_2\text{O} \cdot x(\text{SiO}_2)$ until the region adjacent to the SiO_2 film has the liquidus composition (SiO_2 saturated) and the morphology shown in figure 4(b).

ENTRY CONDITIONS

The chemical reactions which lead to pinhole formation are expected to occur when the shuttle wing leading edges are hottest—during launch and re-entry (ref. 5). Launch lasts about eight minutes and involves temperatures only to about 755 K (900 °F). Re-entry involves temperatures up to 1922 K (3000 °F) and lasts about 30 min. The time to reach temperature is 5 to 8 min and the highest temperatures last about 7 to 8 min. Possible trans-Atlantic (TAL) abort trajectories for the Shuttle involve temperatures to 2095 K. The re-entry atmosphere is essentially a reduced pressure of air—0.005 to 0.010 atm and contains a complex mixture of molecules, atoms, and ions. There is a good deal of information on this atmosphere (ref. 5). Simulating this environment for ground based studies with controlled variables has always been a problem. However an arc-jet is generally accepted as the best approach (refs. 6 and 7).

IMPURITY DEPOSITS

The orbiter may sit on the launch pad for periods of up to a month before launch. The sea-salt laden air of the Florida coast is a corrosive environment to both the launch structure and the vehicle. Recently Gordon (ref. 8) has completed a series of chemical analyses to determine the protected RCC contamination. Most of the impurities found are from the weathering paint. These include Fe, Ca, Si, Zn, Al, Mg.

CONDITIONS FOR PINHOLE FORMATION

After about 10 to 15 flights small pinholes have been observed primarily on the wing leading edge. Detailed descriptions of these pinholes have been reported in several reports (refs. 1 and 9). Here we shall summarize the observations critical to the mechanism. Initially pinholes were discovered on the wing leading edge on each of the four orbiters. Later a small number of pinholes were discovered on the nose-cap. The wings are exposed on the pad, whereas the nose-cap is covered. The orbiter, OV-102 (Columbia), has the largest number of pinholes. This is the oldest of the shuttles and generally flies hotter.

Figure 6 shows six different pinholes from OV-102. Some are from a panel removed after 15 flights and some from a panel removed after 19 flights. For each pinhole, a surface view and a polished cross section is presented. In all cases the surface view is a backscattered electron image (BSE). In some cases a BSE image of the polished cross section is presented; in other cases an optical micrograph of the polished cross section is presented. From these micrographs and other observations, a number of generalizations about pinholes can be made.

In a BSE image, the phases with heavier elements tend to appear brighter. Elemental identification of these bright phases indicated a large amount of zinc. The source of this zinc is likely the flaking paint from the launch structure. Thus pinholes are always associated with zinc. As pointed out by Christensen (ref. 1), the glass adjacent to the pinhole has a more frothy and bubbly appearance than the glass which normally covers the RCC. The BSE images of the cross sections indicate that the zinc-rich glass flows into the pinholes. In addition the pinholes are nearly always along craze cracks in the SiC. These are formed due to the thermal expansion mismatch between the carbon/carbon and the SiC coating. The cross sections all suggest that the pinhole is simply an enlargement of upper portion of one of these cracks.

PROPOSED MECHANISMS

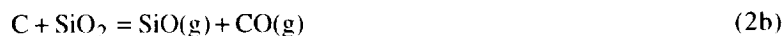
A number of mechanisms have been proposed to explain the pinhole formation (refs. 1, 9 to 11). To date, no mechanism fully explains all of the observations associated with pinholes. The proposed mechanisms have been

nicely summarized in the report by Christensen (ref. 1). Therefore we shall only briefly discuss the key issues of each mechanism, with an emphasis on the high temperature chemical reactions in each process.

Several proposed mechanisms are based on internal effects (refs. 1, 9 and 11). These are shown schematically in figure 7(a) to (c) and listed below:

(a) Pinholes are defects in the SiC coating formed during processing. As the outer layer of glass volatilizes during each mission, these defects are exposed.

(b) Interaction of SiC (or C) and SiO₂ to generate gases:



(c) Formation of SiO(g) due to low partial pressures at the bottom of pinhole and subsequent re-oxidation to SiO₂(s) at the top.

The basic problem with each of these is that they do not account for the concentration of zinc noted at each pinhole. In addition, one would expect mechanism (a) to be operative in laboratory furnace tests. Despite extensive testing of the coated RCC material in the laboratory, no pinholes have been observed.

A sodium chloride induced mechanism was proposed in reference 10. This is shown schematically in figure 8. In this case the NaCl is proposed to collect in a crack or fissure where the oxygen potential is low. This reacts with the SiC to form SiCl_x species—primarily SiCl₂. These diffuse to the top and are re-oxidized to SiO₂, which would create an additional glassy area near the pinhole. As will be shown, sodium chloride is present on the RCC material, very likely from the sea-salt laden air of the cape. It has been shown that this is a thermochemically viable mechanism for pinhole formation and that diffusion can account for the material removal necessary to create these pits (ref. 10). However this mechanism does not account for the concentration of zinc associated with each pinhole and sodium chloride/RCC laboratory tests were not able to reproduce the pinholes or any actual pinhole features. However, non-representative pinholes were formed after treating a coated RCC coupon with sea salt and testing in a NASA/JSC arc-jet (refs. 1 and 13).

The concentration of zinc associated with each pinhole cannot be ignored. It is likely that the zinc plays a role in pinhole formation. Christensen (ref. 1) suggests that formation of various zinc silicate products may indeed lead to consumption of the SiC coating and pinhole formation. In this report we shall build on this idea. A series of microstructures will be examined and discussed to develop a detailed, thermochemically sound mechanism.

EXPERIMENTAL

This report consists of three experimental sections: (1) Detailed microstructural observations of RCC material removed from the Shuttle. (2) Mass spectrometric studies of the RCC material removed from the Shuttle and (3) Laboratory furnace studies of the RCC material and microstructural examination.

(1) Observations from Shuttle

The pinhole cross sectioning technique, illustrated in figure 6, was particularly useful for this study. This has been described in a previous publication (ref. 12) and will only be briefly summarized here. The region around the pinhole was cut with a diamond sectioning saw and then gently polished to reveal a cross section of the pinhole. Samples were examined with both optical and scanning electron microscopy (SEM). As mentioned, backscattered electron (BSE) images were particularly useful in identifying regions containing zinc. A newer SEM with a field emission gun (FEG) was particularly valuable for high magnification examination of the glass/SiC interface. Elemental analysis was done with energy dispersive spectroscopy (EDS). One issue with EDS is the overlapping of the Zn and Na peaks. Additional elemental analyses were therefore done with a wavelength dispersive spectrometer (WDS), which allowed separation of the Na and Zn peaks.

(2) Mass Spectrometric Studies of the RCC Shuttle Material

When an RCC panel from the shuttle was tested in the NASA JSC arc-jet facility, a red-orange gas emerged from the pinholes was observed (ref. 13). This is shown in a video captured photograph in figure 9. Identifying this gas has proven to be a challenge. Classical methods of gas identification (e.g., mass spectrometry and UV/VIS/IR based spectroscopies) are simply not possible in an arc-jet. Caution should be taken in interpreting the colors in figure 9, however the red-orange appearance is strongly suggestive of a sodium flame spectra.

We examined these same types of panels in our molecular beam mass spectrometer at NASA Lewis. This unique instrument allows direct mass spectrometric sampling of a process occurring at one atmosphere with a high sensitivity quadrupole mass spectrometer. This is accomplished by a free-jet expansion of the gases to be sampled into a large, rapidly pumped vacuum chamber. This leads to a well-defined molecular beam with limited molecule/molecule and molecule/wall collision. The beam is directed to a mass spectrometer in an ultra-high vacuum chamber and chemical and dynamic integrity of the sampled gas is preserved. A block diagram of this system is shown in figure 10 and more details on the system can be found in reference 14. This particular configuration is well-suited to identifying high temperature, condensable species such as NaCl(g) , Zn(g) , and $\text{Na}_2\text{O(g)}$. The sensitivity is better than one ppm.

(3) Laboratory Furnace Tests

Although duplicating the complex conditions of vehicle re-entry in a laboratory furnace is not possible, we can examine some possible RCC/ZnO/entry atmosphere reactions at elevated temperatures in the laboratory. It is important to note the Zn from the paint would not exist in elemental form, but rather as a binary oxide or complex oxide. For these studies we used ZnO. Table I lists the various reactants and furnace exposures used. In order to put ZnO on a SiC or RCC coupon, a water-based slurry of ZnO was made. Drops of this slurry were put on the coupon and the coupon then dried in a drying oven at 100 °C for several hours. Then the specimen was heat treated under the conditions given in table I. After exposure, samples were analyzed in several ways. SiC samples were chemically analyzed after treating in warm 10 percent HF for 2 hr to remove the reaction products. These products were then analyzed with atomic emission spectroscopy. In addition, standard scanning electron microscopy was used to examine the sample surfaces and cross sections. Electron microprobe analysis (EPMA—JEOL Superprobe, Binghamton University, Binghamton, NY) was used for determining elemental distributions.

RESULTS

Pinhole Microstructures

In this section, we present detailed microstructural examinations of the pinholes shown in figure 6. Figure 11 is a high magnification micrograph and associated EDS of figure 6(a). This was taken in the backscattered mode with our FEG-SEM. Note that the Na-Zn-Si-O glass only extends to the bottom of the enlarged crack. Below this, only a Na-Si-O glass is observed in the crack. Figure 12 is a 7000X magnification of a region of the glass in the enlarged part of figure 6(f). Three distinct layers are present in the glass and associated EDS spectra show a gradient in Zn. The inner most layer is nearly pure silica. The EDS spectra indicate a gradient in Zn concentration through the layers with the largest concentration on the outside. As discussed, Na and Zn peaks overlap in EDS spectra. In order to resolve these, WDS was taken of this glassy region. The SEM with the WDS attachment did not allow the three layers to be resolved. However a WDS spectrum of the entire glass region showed both Na and Zn (fig. 13). Typically such SiO_2 dissolution microstructures (ref. 2) show a pure layer of SiO_2 adjacent to the SiC and a decreasing gradient in Na from the gas/solid interface. Further, in this case, it is likely that both Na and Zn show similar gradients, decreasing toward the SiC/glass interface.

Mass Spectrometry of Shuttle RCC Panels

As discussed, we could not attach a mass spectrometer directly to an arc-jet. However, we could very roughly approximate the conditions of the arc-jet in our high pressure sampling mass spectrometer. To do this, we used a

mixture of 1 percent oxygen/Ar and heated the sample to 1100 °C. Interestingly, the mass spectrum showed a lot of Zn and NaCl vapors. This is shown in figure 14. These vapors were observed for about 5 to 10 min at temperature. Unfortunately, we were not able to view the samples during this test, so we cannot unequivocally say that the orange-red gas was Zn(g) and/or NaCl(g). However this test indicated there was a substantial amount of Zn and NaCl deposited on the RCC panels.

Furnace Tests of SiC and RCC Panels

A limited number of furnace tests were done to try to understand some of the high temperature reactions. The conditions are listed in table I. The results of a simple test of ZnO and SiC are illustrated in figure 15 and listed in table II. It appears that ZnO enhances the oxidation of SiC by a factor of two. This is very likely by the Zn doping the SiO₂ network and leading to faster transport rates. Since the ZnO-SiO₂ eutectic is high (fig. 16—1705 K), no liquid is formed under these conditions. A solid system exhibits much less attack than a liquid system.

Some tests were also done on the RCC material + ZnO. In this case extensive reaction was noted, as shown in the optical micrographs in figure 17. This bubbly, friable glass was reminiscent of the glass observed on the shuttle specimens. This glass was further examined with the EPMA. First a region which appeared to be Zn-rich glass on SiC was examined. This is shown in figures 18 and 19. These figures indicate a thick layer of Zn-rich glass, with a thin layer of SiO₂ adjacent to the sample. The large bubble indicates extensive gas generation. Figure 19 shows an enlarged region with what are very likely SiO₂ crystallites adjacent to the SiC. This is reminiscent of the glass observed on the shuttle specimens.

Figure 20 a region where the Zn-rich glass was adjacent to a SiO₂ filled region. This SiO₂ region was likely formed in processing by the TEOS vacuum infiltration/decomposition to silica step. The significant point here is that the zinc rich glass maintains a distinct layer from the silica.

In order to explore the effects of both ZnO and NaCl on the RCC material, a coating of NaCl was put on the Zn-rich glass. The EPMA results are shown in figure 21. Generally most of the NaCl remains on top of the ZnO-rich glass with little interaction. However the elemental maps suggest that some Cl flows down a crack.

DISCUSSION

It is appropriate to summarize what we know about pinholes at this point:

A. Shuttle:

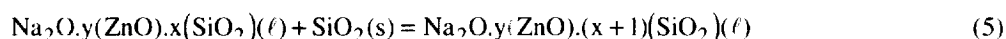
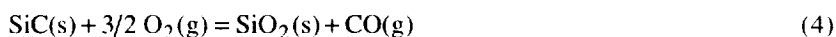
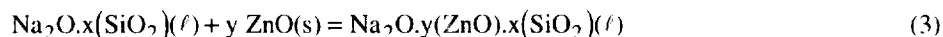
1. Pinholes form on primarily on the wing leading edges, but not necessarily on the hottest parts.
2. A minimal amount of pinholes form on the nose cap, which is covered while on the launch pad.
3. Pinholes appear after 10-15 flights.
4. The orbiter may sit on the pad up to a month, collecting various impurities from flaking paint and the sea salt laden air. The frequent appearance of zinc appears to be highly significant.
5. Mass spectrometric evidence indicates Zn and NaCl collect on the coated RCC material.
6. Pinholes are associated with a region of zinc rich glass.
7. The zinc rich glass appears frothy and more fluid than the Type A glass.
8. Pinholes occur along the cracks in the SiC caused by CTE mismatch between the RCC and the SiC coating.
9. Pinholes appear to be an enlargement of the outermost regions of the cracks in the SiC.
10. Detailed microstructural examination of the glass inside the pinholes indicates an Na-Zn-Si-O glass with multiple composition layers. There is a decreasing gradient in Zn and Na toward the glass/SiC interface with nearly pure SiO₂ crystallites adjacent to the SiC.

B. Laboratory Experiments:

1. ZnO does not react appreciably with pure SiC.
2. ZnO appears to cause a vigorous reaction with the protected RCC material (Type A glass). This is evidenced by the formation of entrapped bubbles and a thick glassy layer.

3. The glassy Zn-rich layer is not in direct contact with the SiC, rather there is layer of pure SiO₂ crystallites between the Zn-rich glass and the SiC coating on the RCC.
4. NaCl deposits on the glass do not appear to interact with the glass directly.
5. NaCl deposits may collect in internal cracks.

These observations support a zinc oxide based pinhole mechanism and to a less extent a NaCl-based mechanism discussed in an earlier report (ref. 10). Consider the zinc oxide based mechanism. The key observation here is in figure 17. The presence of ZnO on the protected RCC material leads to the formation of a thick Zn-Na-Si-O glass, with a lot of entrapped bubbles. The additional silica in this glass cannot be from the silica which is already a part of the RCC material, but rather must come from oxidation of the SiC layer. This leads to consumption of the layer and also accounts for the extensive gas and resultant bubble formation. Thus a sequence of reactions is likely:



Reaction (3) is significant since it leads to melt with a higher capacity to dissolve silica. The Na-Zn-Si-O compound is likely to be even lower melting than Na-Si-O melts, as can be seen in the Na₂O-ZnO-SiO₂ ternary phase diagram (fig. 22). This lower melting point explains the observed increased fluidity of the glass. Unfortunately due to the formation of glasses of varying stoichiometry, it is not possible to write exact reactions. Note that at the temperatures of reaction, the glass must be molten. Although post-examination has revealed zinc silicates (ref. 1), it is likely that these crystallized out of the melt on cooling.

Figure 23 is a schematic of a proposed mechanism. ZnO particles lodge near existing cracks. Then a Na₂O · y(ZnO) · x(SiO₂) glass forms due to reaction of the ZnO with the sodium silicate sealant via reaction (3). This reactive glass can dissolve the stable SiO₂ layer on the SiC in the crack via reaction (5). Further rapid oxidation of SiC can occur via transport through the Na₂O-ZnO-SiO₂ liquid via reaction (4). This oxidation and dissolution effectively leads to consumption of SiC and enlargement of the crack. In time the Na₂O-ZnO-SiO₂ liquid will become saturated in SiO₂ and the reaction will stop. This type of oxidation and dissolution has been discussed in the introduction and is commonly observed in high temperature Na₂O-induced corrosion reactions (ref. 2 and fig. 4).

However dissolution/oxidation cannot account for the enlargement of cracks to the point of 0.1 mm pinholes. It is proposed during re-entry, fresh surfaces SiC are continually exposed for attack by the Na₂O-ZnO-SiO₂ liquid. The volatile species escaping from the crack (eg. CO(g), NaCl(g), Na₂O(g)) may push out the SiO₂-saturated Na₂O-ZnO-SiO₂ liquid. This process may in fact be the eruptions observed (figure 9 and ref. 13) in the arc-jet testing. In addition, the thermal expansion mismatch between the SiC and the RCC material creates stresses which keep the crack opening and exposing SiC surfaces. Then SiO₂-depleted Na₂O-ZnO-SiO₂ liquid may attack these SiC surfaces. This continual process of oxidation and dissolution (reactions 4 and 5), leads to effective crack enlargement into a pinhole.

RECOMMENDATIONS

It appears that the pinhole formation is a result of external corrosive elements. Most of the evidence points toward the deleterious effects of Zn although NaCl may still play a role. The aging launch structure in the corrosive marine environment is the problem here. Thus the obvious solutions are: physical protection of the wings and improvement of the paint on the launch structure.

The current refurbishment procedure involves sanding off the glass/SiO₂ outer layers on the protected RCC, re-infiltrating with TEOS, decomposing the TEOS to SiO₂, and sealing with Type A glass. This should be adequate for near-term repairs as it will remove the Zn deposits. However, in the long term, pinholes will continue to form and existing pinholes may grow and simply be filled with SiO₂ as long as there is a source of Zn contamination.

This will gradually increase the volume fraction of SiO_2 in the SiC coating, eventually leading to an inadequate coating. Kinetic data would be helpful in assessing how quickly these pinholes form and grow.

In terms of solutions, the removal of the Zn contamination is clearly a needed step—by improved coatings of the launch structure. It is recommended that the quality of the SiC coating should be monitored and the entire RCC material should be replaced periodically. Also development of more crack-resistant coatings (e.g., graded SiC) and corrosion resistant sealants should be beneficial.

SUMMARY

In this report we explore a number of issues related to the observed pinholes in the wing leading edge of the space shuttle. Experimentally this involves (1) Detailed microstructural examination of the pinholes from the shuttle. (2) Mass spectrometric examination of the protected RCC material removed from the shuttle and (3) Laboratory furnace studies to understand ZnO/protected RCC interactions. Most of the evidence points toward a critical role of Zn in creating the pinholes. A mechanism is proposed based on the formation of a $\text{ZnO-Na}_2\text{O-SiO}_2$ ternary glass. This glass runs into cracks and attacks the SiC walls. This effectively enlarges the uppermost portions of the cracks, leading to the observed pinholes. The features of this mechanism are consistent with most of the observations regarding pinholes.

REFERENCES

1. S.V. Christensen, "Reinforced Carbon/Carbon Pin Hole Formation through Zinc Oxide Attack," Rockwell International Internal Letter, RDW-96-057, May 1996.
2. N.S. Jacobson, "Corrosion of Silicon-Based Ceramics in Combustion Environments," *J. Am. Ceram. Soc.*, 76 [1], pp. 3–28, 1993.
3. E.M. Levin, C.R. Robbins, and H.F. McMurdie, Phase Diagrams for Ceramists, The American Ceramic Society, Columbus, OH, 1964, p. 94.
4. M.I. Mayer and F.L. Riley, "Sodium-Assisted Oxidation of Reaction Bonded Silicon Nitride," *J. Mater. Sci.* 13, pp. 1319–28 (1978).
5. Leading Edge Structural Subsystems (LESS) Entry Heating Study—Final Report, Volume—Methodology and Results. Prepared by Lockheed Engineering and Sciences Company, Houston, TX, Contract NAS 9–17900, LESC-30453, May 1993.
6. S.D. Williams, D.M. Curry, D. Chao, and V.T. Pham, "Analysis of the Shuttle Orbiter Reinforced Carbon-Carbon Oxidation System, NASA TM–104792, June 1994.
7. S.D. Williams, D.M. Curry, D.C. Chao, and V.T. Pham, "Ablation Analysis of the Shuttle Orbiter Oxidation Protected Reinforced Carbon-Carbon," Paper AIAA 94–2084, presented at the 6th AIAA/ASME Joint Thermophysics and Heat Transfer Conference, June 20–23, 1994, Colorado Springs, CO.
8. M. Gordon, private communication
9. D.W. Johnson, Final Report—RCC Pin-hole/Sealant Loss Investigation, Lockheed Martin 221RP10558, September 1996.
10. N.S. Jacobson and R.A. Rapp, "Thermochemical Degradation Mechanisms for the Reinforced Carbon/Carbon Panels on the Space Shuttle," NASA TM–106793, January 1995.
11. J.A. Orench, "A Mechanism of Pinhole Formation in the Reinforced Carbon-Carbon Thermal Protection System of the Space Shuttle Orbiter," MS Thesis, College of Engineering, University of Central Florida, 1996.
12. N.S. Jacobson, T.A. Leondhardt, D.M. Curry, and R. A. Rapp, "Oxidative Attack of Carbon/Carbon Substrates through Coating Pinholes," *Carbon* in press.
13. D.M. Curry, private communication.
14. C.A. Stearns, F.J. Kohl, G.C. Fryburg, and R.A. Miller, "A High Pressure Modulated Molecular Beam Mass Spectrometric Sampling System," NASA TM–73720, 1977.
15. Op. Cit. Levin, p. 120.
16. E.M. Levin and H.F. McMurdie, Phase Diagrams for Ceramists 1975 Supplement, The American Ceramic Society, Columbus, OH, 1975, pp. 206–207.

TABLE I. LABORATORY SAMPLES AND EXPOSURE CONDITIONS.

Material	Designation	Deposit	Gas atmosphere	Temperature, °C	Pressure, atm	Times, hr
SiC	SiC 4, 5		Air	1000	0.007	1
	SiC/ZnO 2,3	ZnO	Air	1000	0.007	1
	CVD SiC 1, 2, 3		Air	1200	0.007	1
	SiC/ZnO-12-1, 2, 3	ZnO	Air	1200	0.007	1
	CVD SiC A, B, C		Air	1450	0.007	1
	CVD/ZnO A, B, C	ZnO	Air	1450	0.007	1
Protected RCC	PC-1	ZnO	Air	1200	1	27x 0.5 hr cycles
	C-1	ZnO NaCl added after four cycles	Air	1200	1	4x 0.5 hr cycles
	CC-ZnO-12-C-1	ZnO	Air	1200	0.092	2x 0.5 hr cycles
	CC-ZnO-1-2	ZnO	Air	1000	0.092	2x 0.5 hr cycles
	CC-ZnO-2-1	ZnO	Air	1200	0.092	1x 0.5 hr cycles

Table II. XRD and chemical analysis results for ZnO + SiC study.

Sample	XRD Results	Weight of products, mg	Si, mg	Zn, mg
SiC Oxidation at 1000°C				
SiC 4		0.2	20	
SiC 5		0	15	
SiC + ZnO Oxidation at 1000°C				
SiC/ZnO 2	SiC, ZnO, Zn ₂ SiO ₄	18.3	40	15.74
SiC/ZnO 3	SiC, ZnO, Zn ₂ SiO ₄	18.8	40	16.18
SiC Oxidation at 1200°C				
SiC 1	SiC			
SiC 2		0.1	55	
SiC 3		0.2	27.5	
SiC + ZnO Oxidation at 1200°C				
SiC/ZnO-12-1	SiC, SiO ₂ , Zn ₂ SiO ₄			
SiC/ZnO-12-2		1.4	145	1.1
SiC/ZnO-12-3		2.3	130	1.96
SiC Oxidation at 1450°C				
SiC A	SiC, SiO ₂ (α-cristobalite)			
SiC B		0.2	127.5	
SiC C		0.3	155	
SiC + ZnO Oxidation at 1450°C				
SiC/ZnO A	SiC, SiO ₂ (α-cristobalite)			
SiC/ZnO B		0.4	265	0.5
SiC/ZnO C		0.2	247.5	0.25

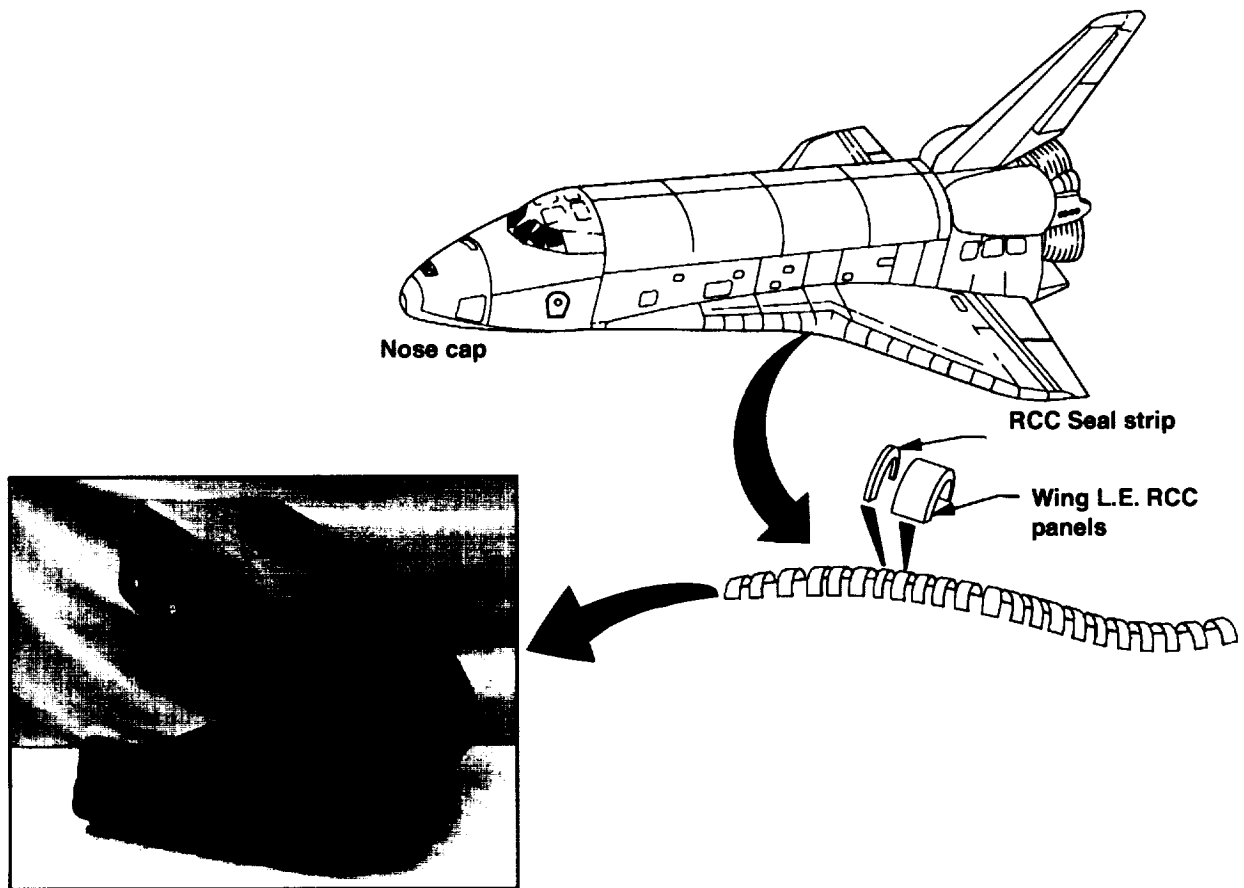


Figure 1.—Schematic of shuttle showing RCC panel location.

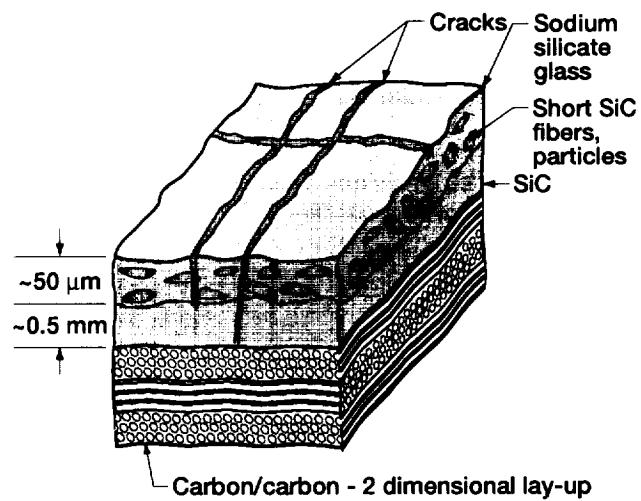


Figure 2.—Diagram of material.

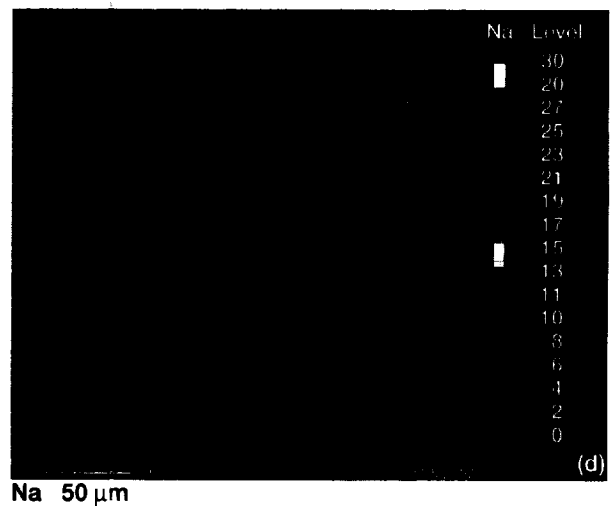
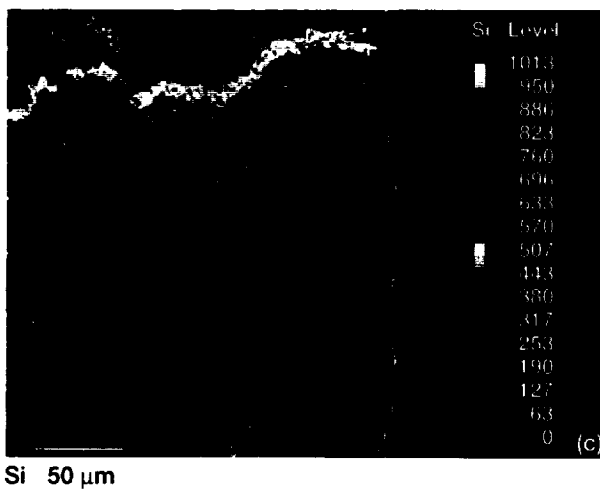
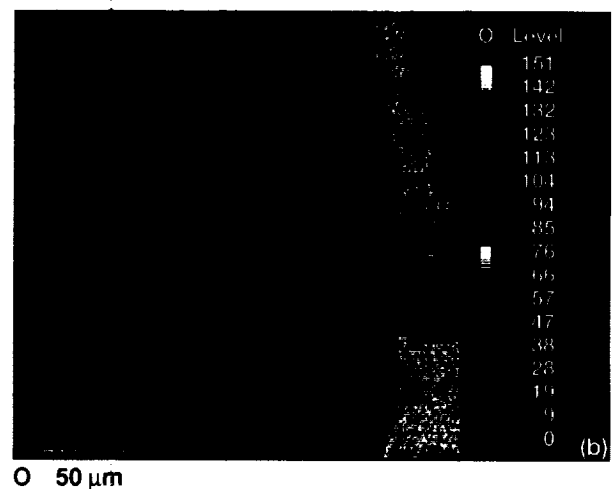
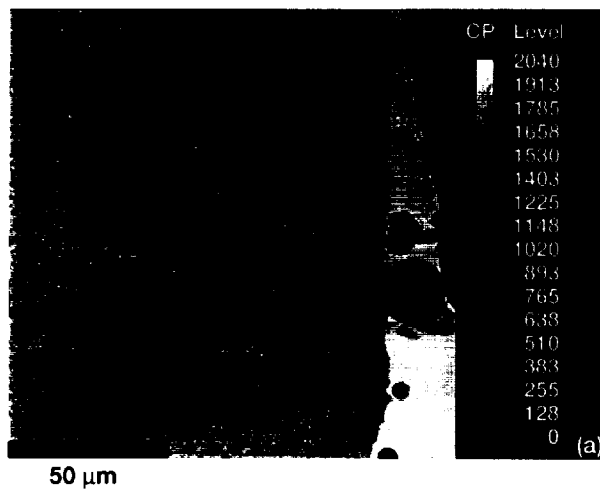


Figure 3.—Cross section of material, BSE image and associated oxygen WDS map, illustrating a crack formed as-fabricated (filled with SiO_2) and in-service (not filled).

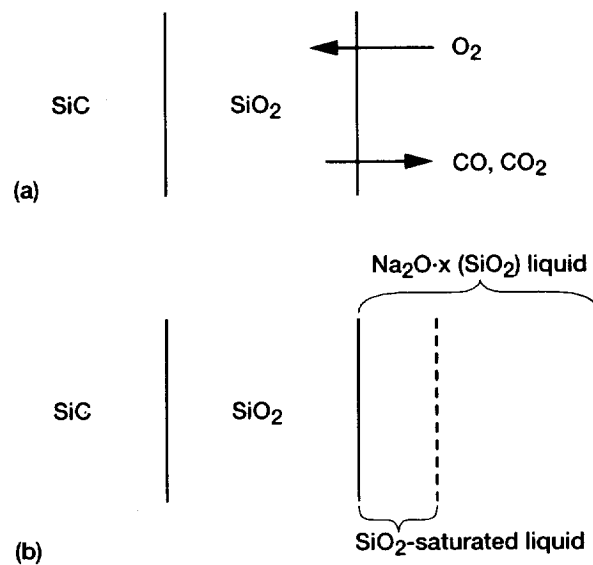


Figure 4.—Diagram of (a) SiC oxidation process and (b) thermochemically stable Na₂O·x (SiO₂) coating on SiC.

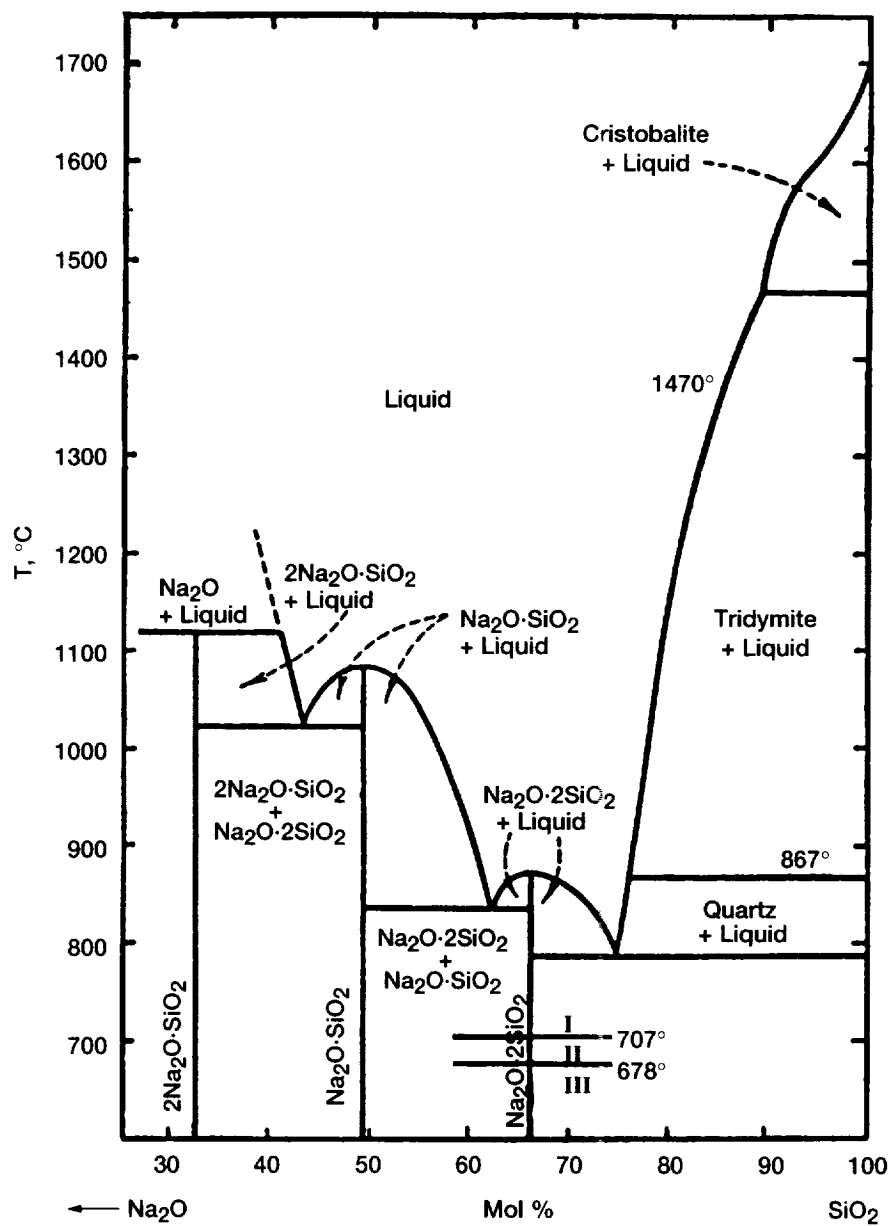


Figure 5.—Na₂O-SiO₂ binary phase diagram (ref. 3).

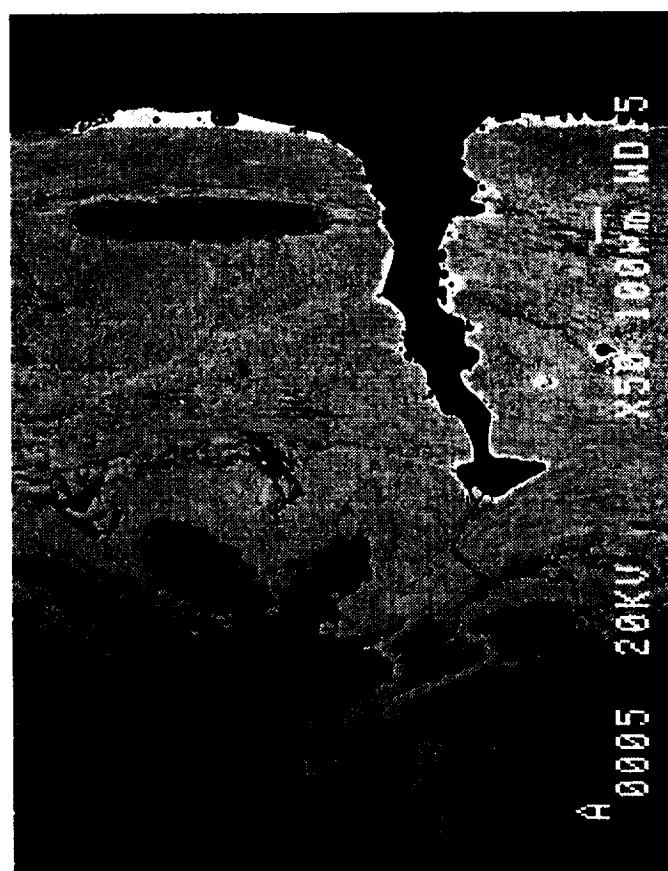
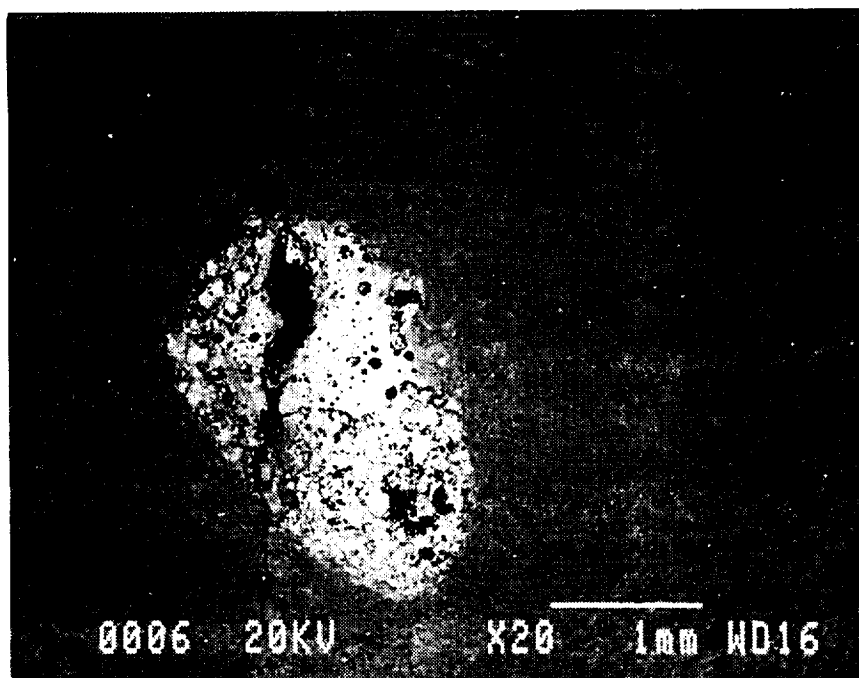


Figure 6.—(a) Pinhole from OV-102, Wing Leading Edge Panel 12 RH, 15 flights.
Cross-sectional view is a BSE micrograph.

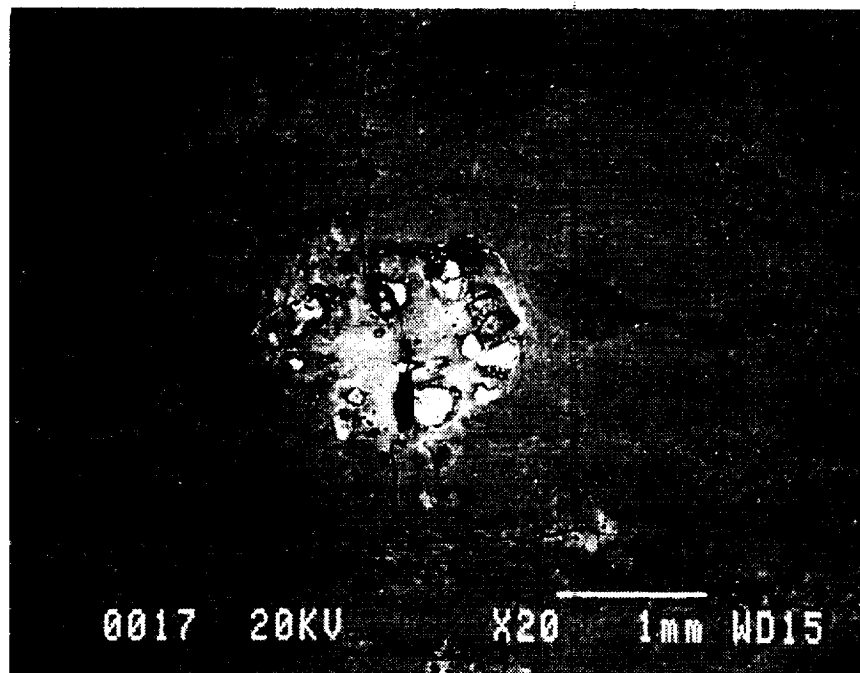


Figure 6.—Continued. (b) Pinhole from OV-102, Wing Leading Edge Panel 12 RH, 15 flights. Cross-sectional view is an optical micrograph.

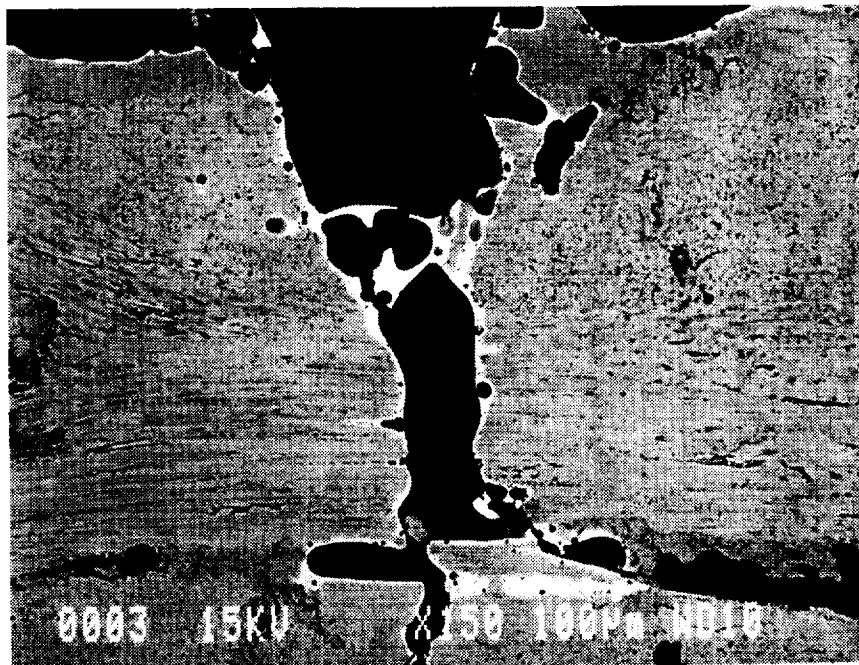
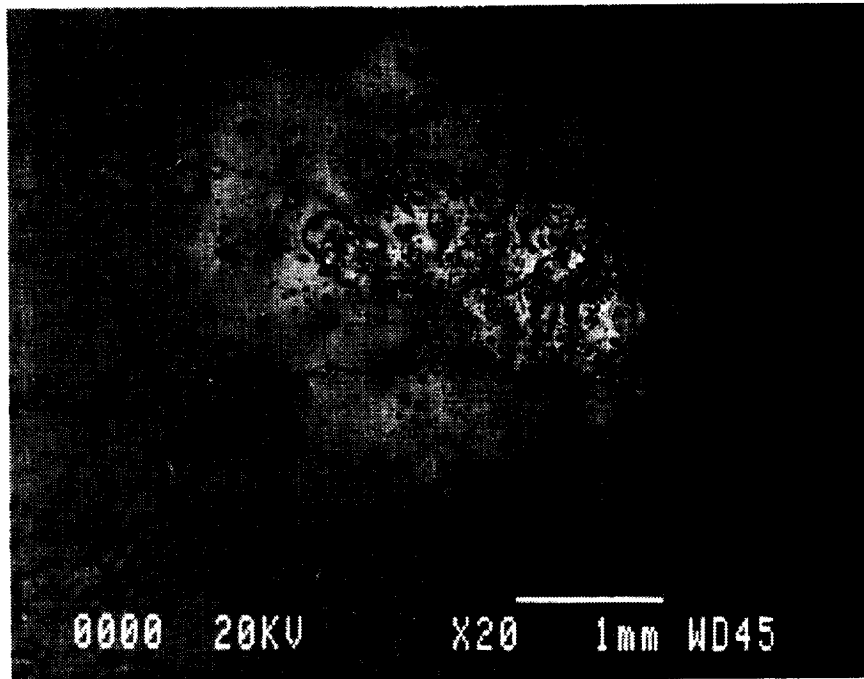


Figure 6.—Continued. (c) from OV-102, Wing Leading Edge Panel 10 LH, 19 flights. The cross-sectional view is a BSE micrograph.

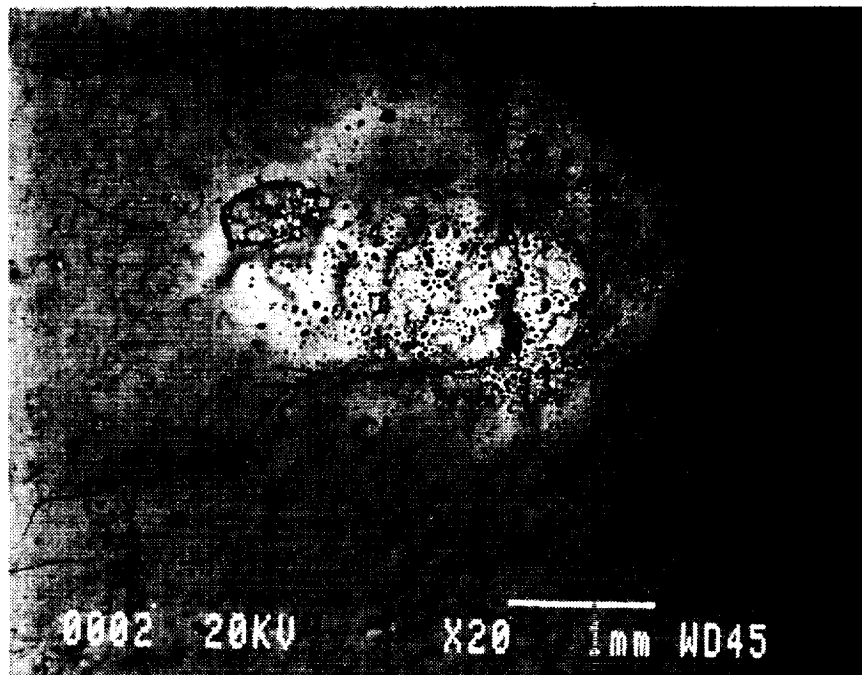


Figure 6.—Continuing. (d) from OV-102, Wing Leading Edge Panel 10 LH, 19 flights. The cross-sectional view is a BSE mic ograph.

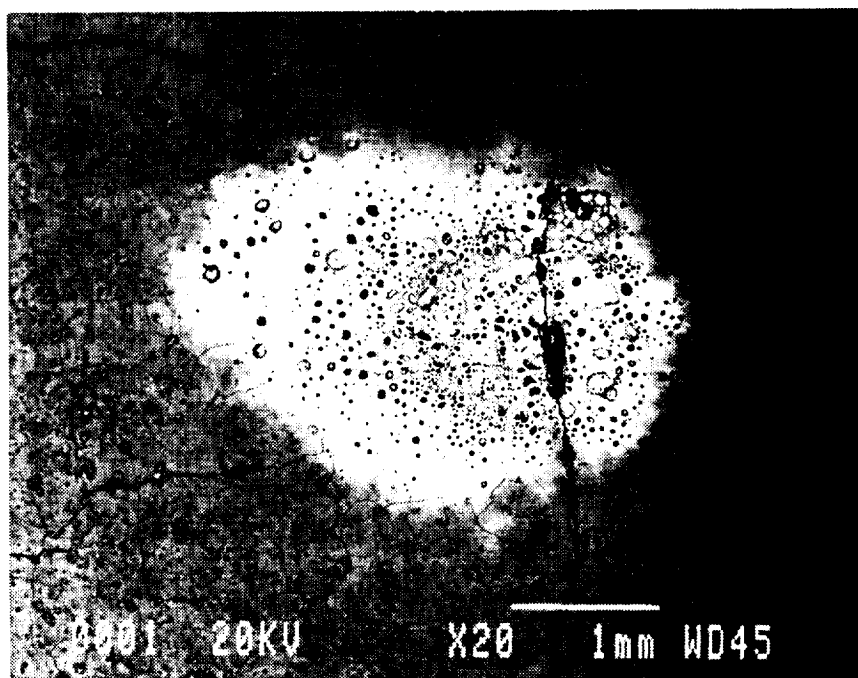


Figure 6.—Continued. (e) from OV-102, Wing Leading Edge Panel 10 LH, 19 flights. The cross-sectional view is an optical micrograph.

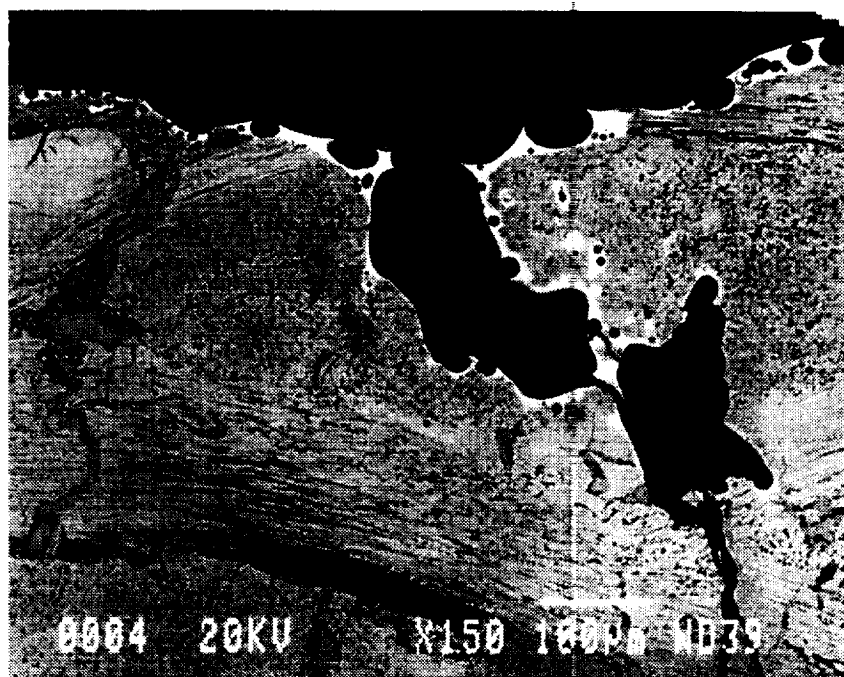
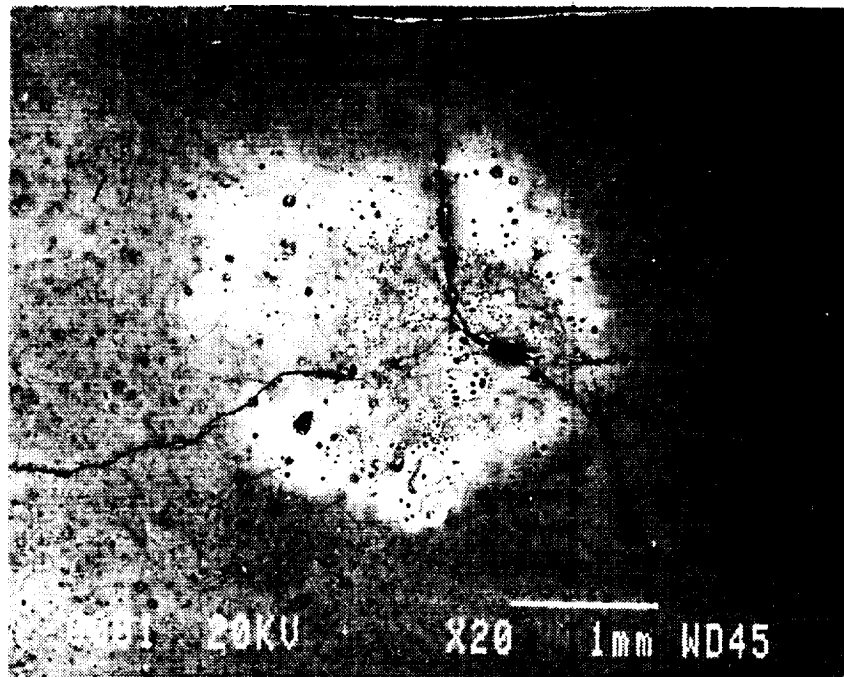


Figure 6.—Continued. (f) from OV-102, Wing Leading Edge Panel 10 LH, 19 flights. The cross-sectional view is a BSE micrograph.



Figure 6.—Concluded. (g) Figures from OV-102, Wing Leading Edge Panel 10 LH, 19 flights. The cross-sectional view is a BSE micrograph.

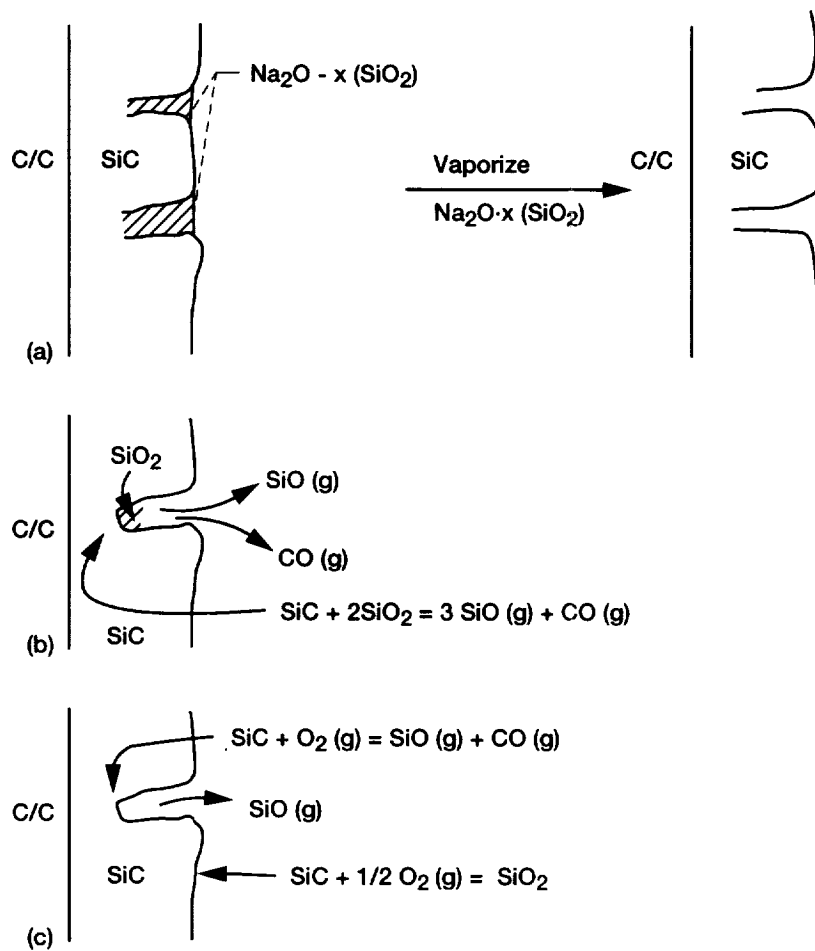


Figure 7.—Schematic of proposed pinhole formation mechanisms which are intrinsic to the material.

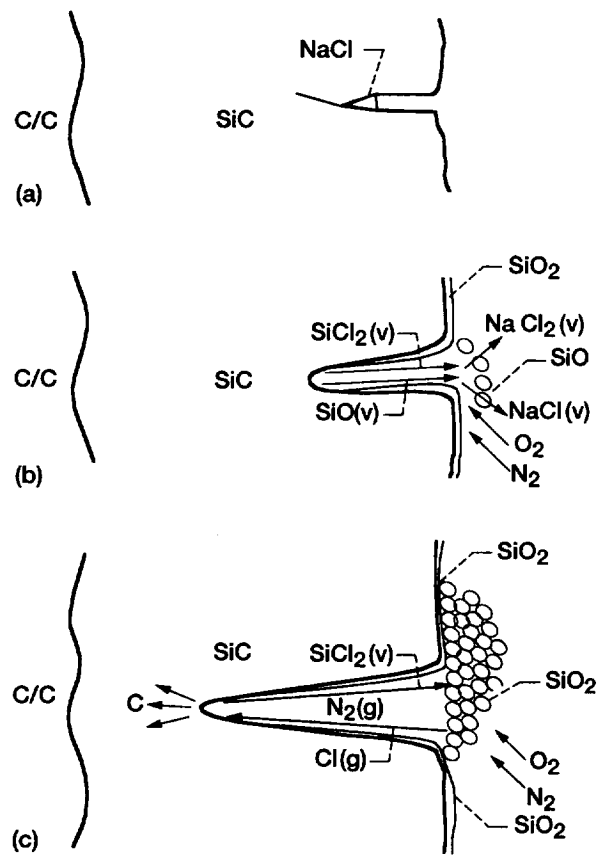


Figure 8.—Schematic of the proposed NaCl pinhole formation mechanism (ref 10).



Figure 9.—Photograph (video captured) of orange-red gas emerging from pinholes in an arc-jet test.

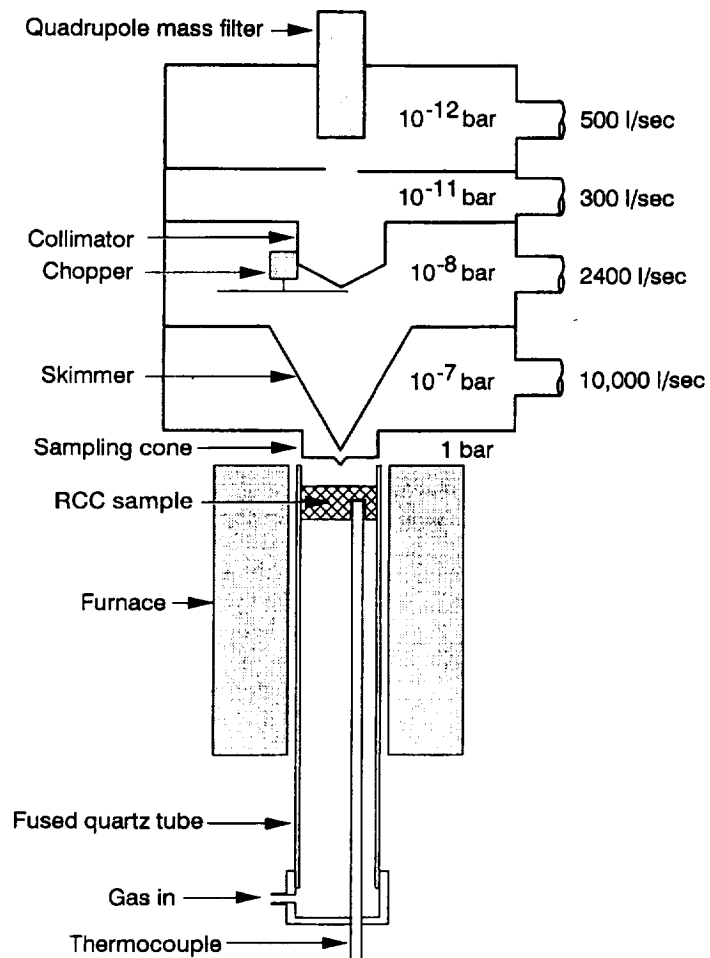


Figure 10.—Schematic of molecular beam mass spectrometer.

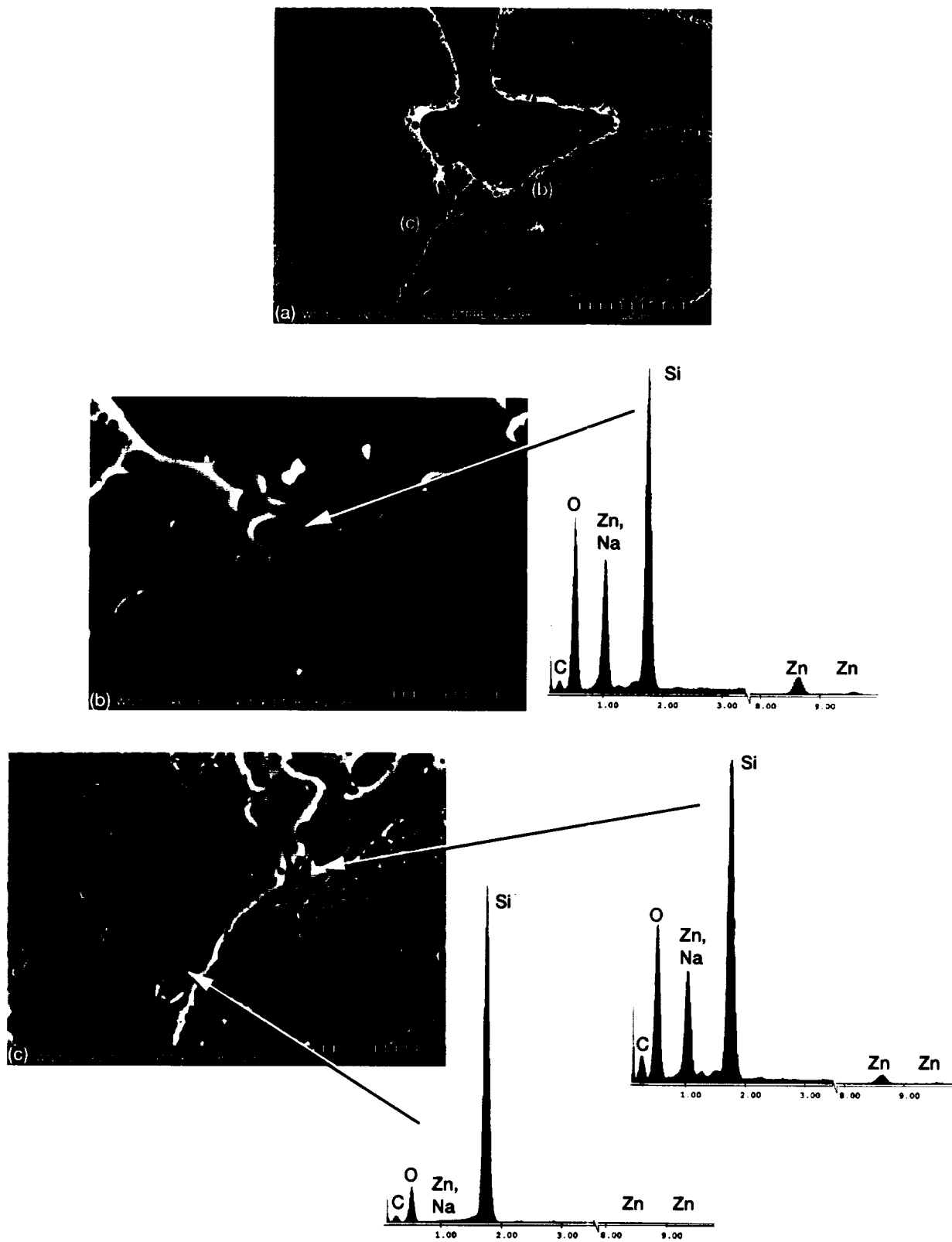


Figure 11.—(a) High magnification of photo of glass/SiC interface in a pinhole (full view is in Figure 6(a)) and associated EDS traces with regions (b) and (c). Note that Zn only extends to bottom of enlarged portion of crack.

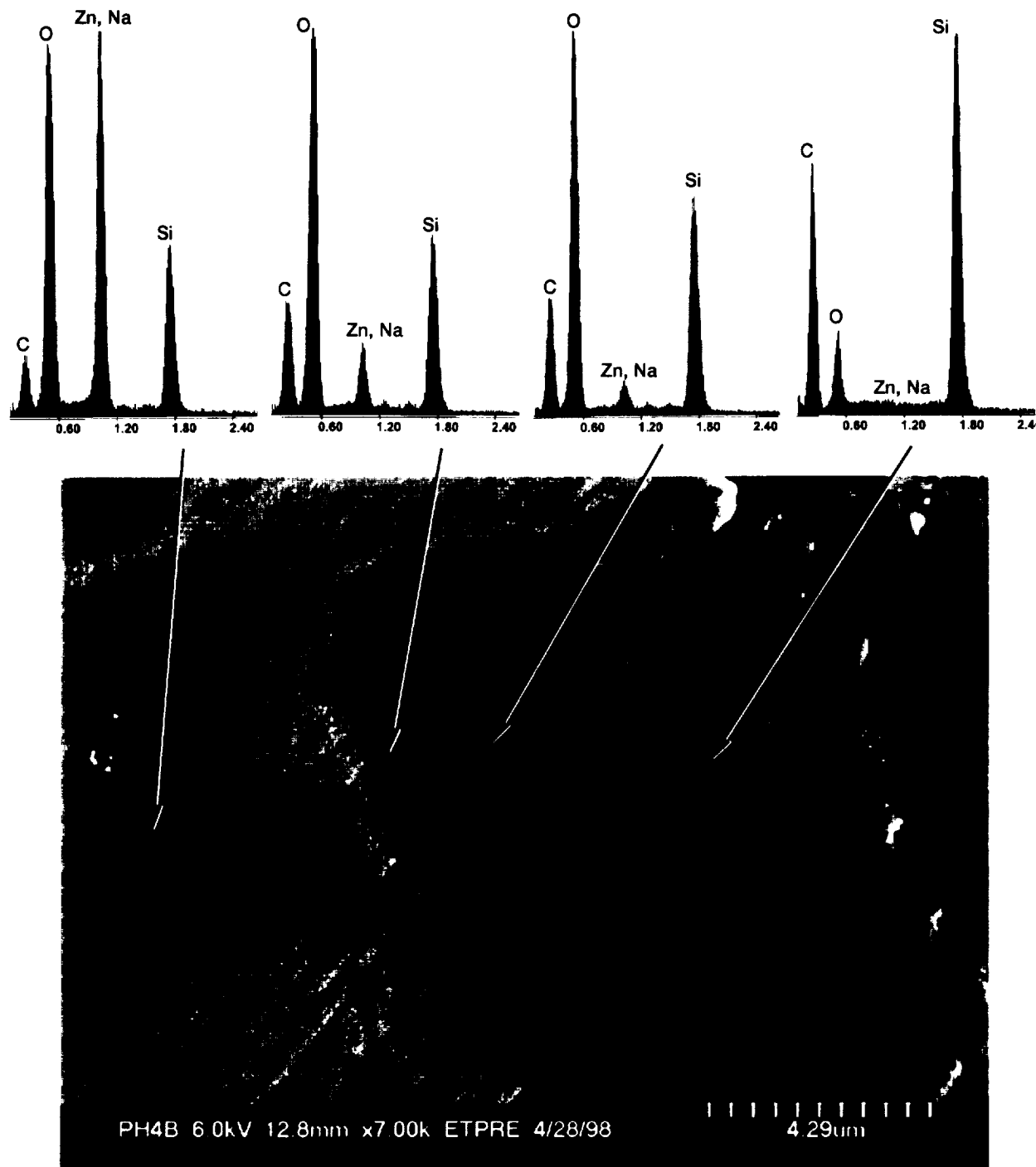


Figure 12.—High magnification photo of the glass/SiC interface in a pinhole (Figure 6(f)), showing composition at various points within the pinhole.

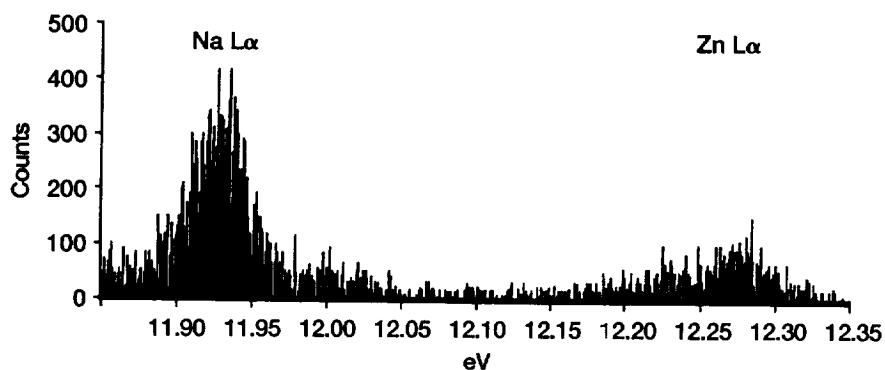


Figure 13.—WDS of the pinhole glass, indicating it is rich in both Na and Zn. This resolves the signal EDS peak in Figure 11 & 12.

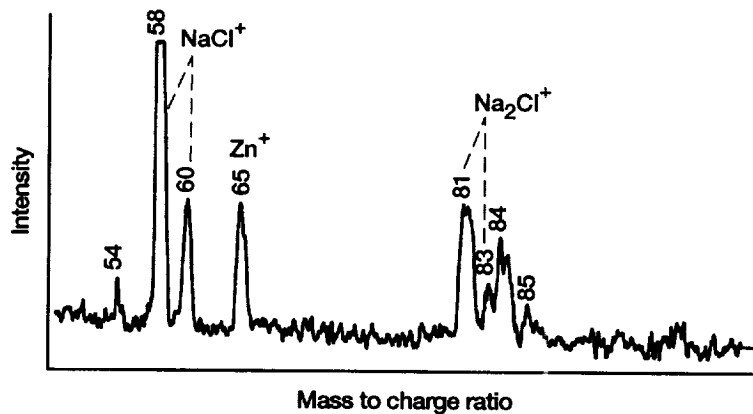


Figure 14.—Mass spectrometer trace showing gases coming off protected RCC removed from the shuttle. The trace indicates the presence of both NaCl(g) and Zn(g).

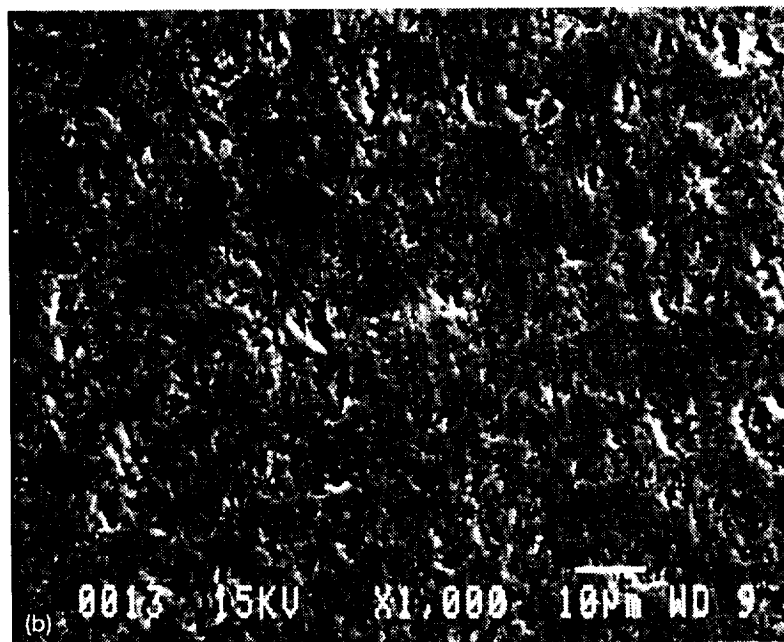
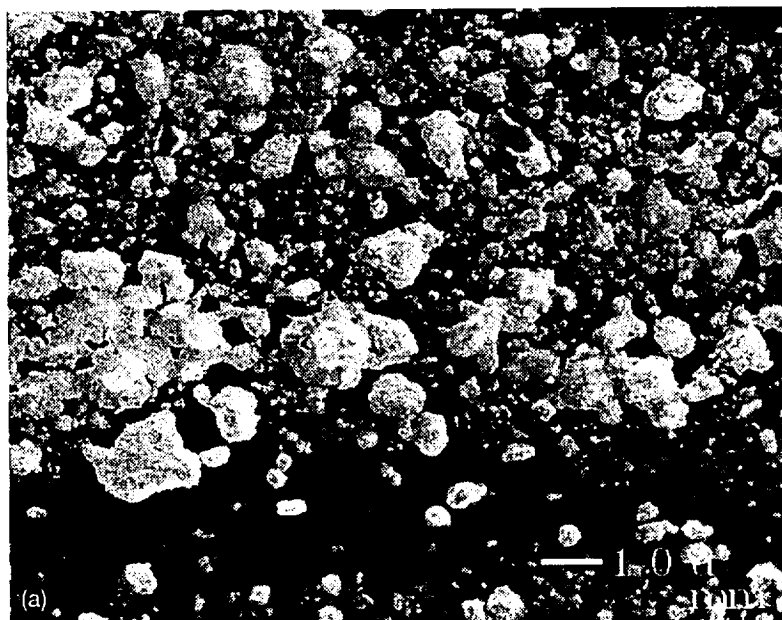


Figure 15.—CVD SiC with ZnO, 1 hr in 0.05 atm air. (a) Surface view showing ZnO and Zn_2SiO_4 on surface after 1000 °C treatment. (b) Surface product in 14(a) removed by treatment in aqueous HF solution to reveal limited surface attack after 1200 °C treatment.

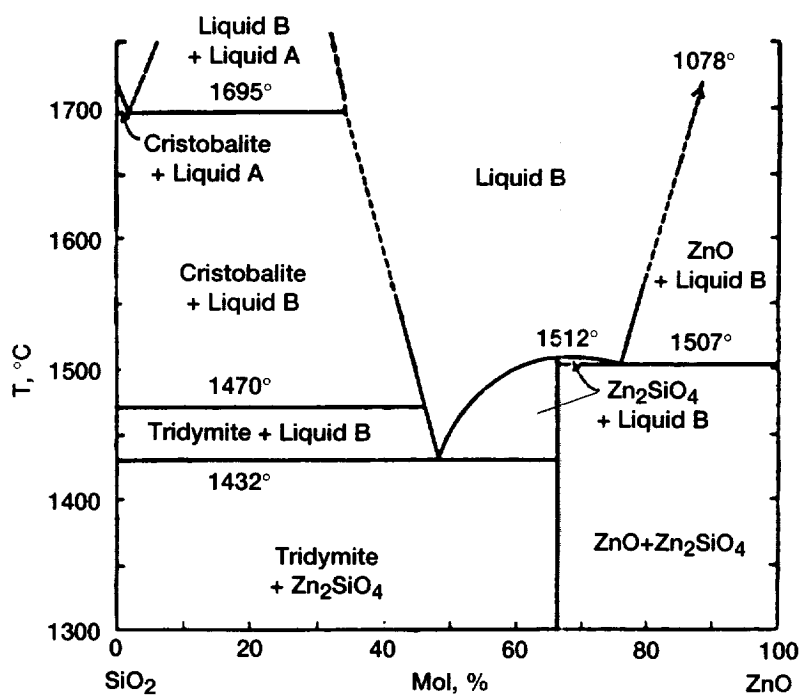


Figure 16.—ZnO-SiO₂ binary phase diagram (ref. 15).

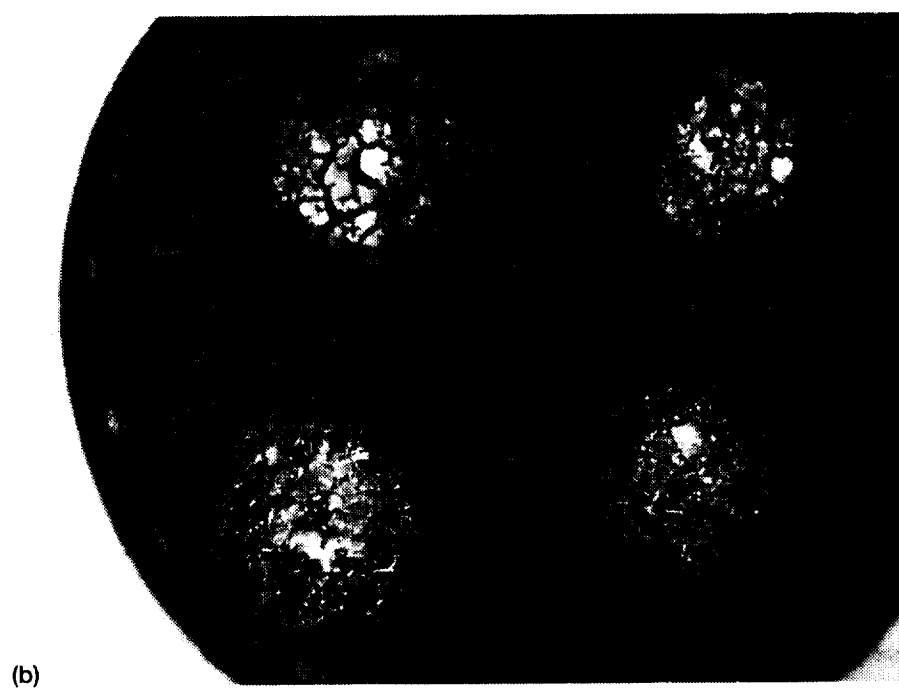
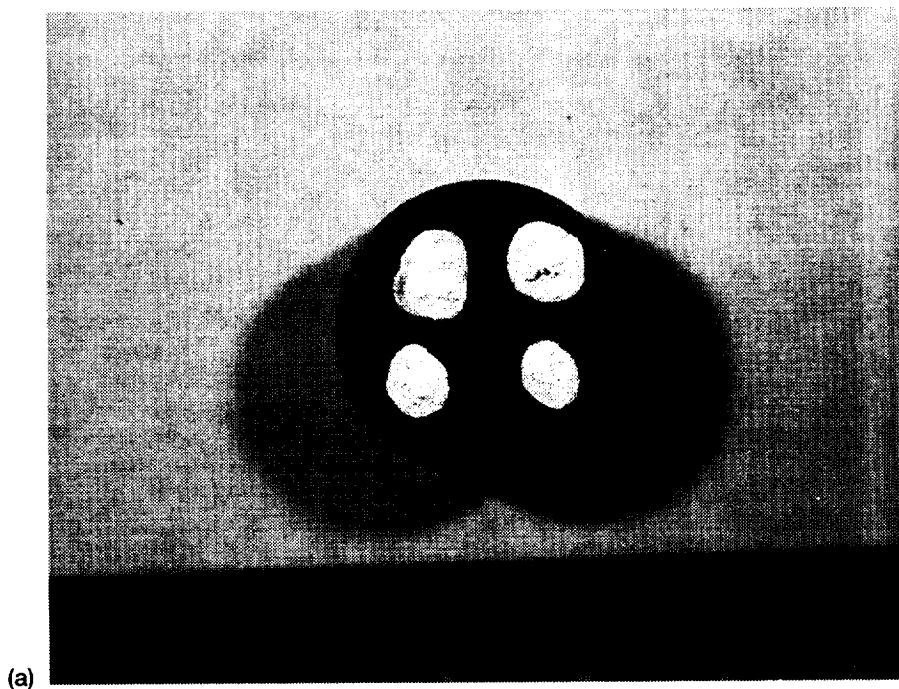


Figure 17.—Protected RCC material and ZnO (a) Before reaction. (b) After 1 cycle in 0.092 atm air for 0.5 hr at 1200 °C.

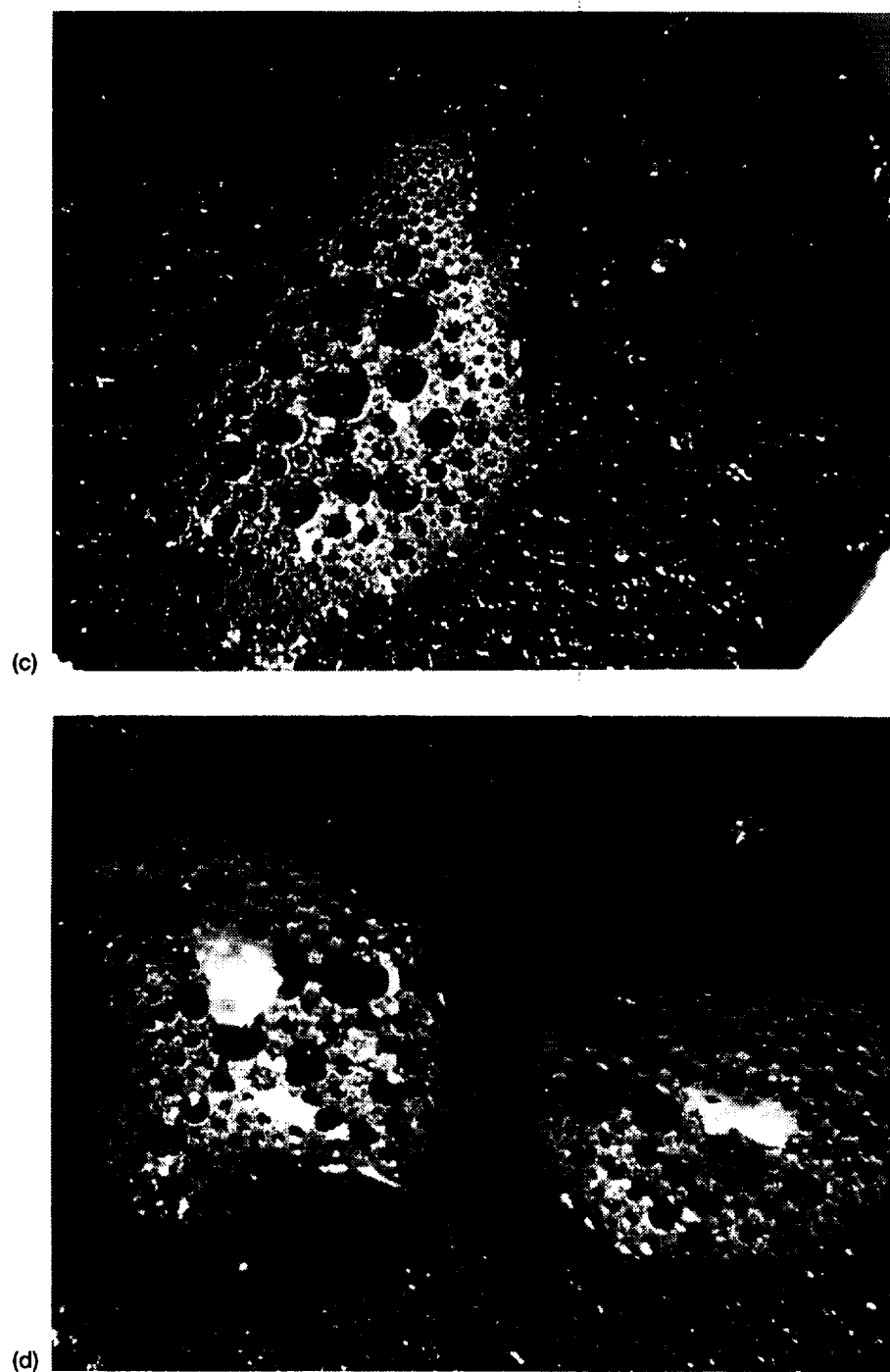
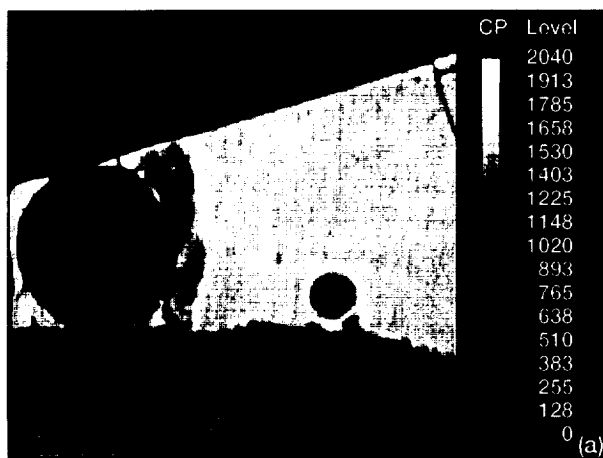
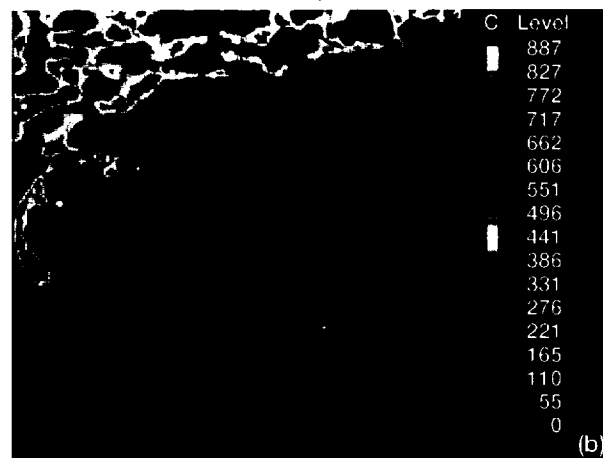


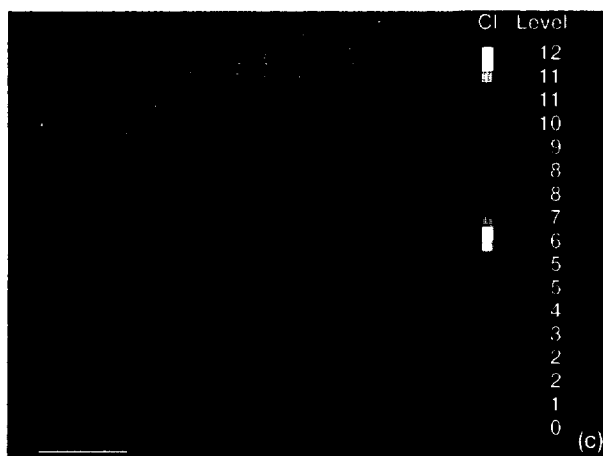
Figure 17.—Concluded. (c) After 4 cycles in 1 atm air. (d) After 27 cycles in 1 atm air. These cycles are 0.5 hr at 1200 °C.



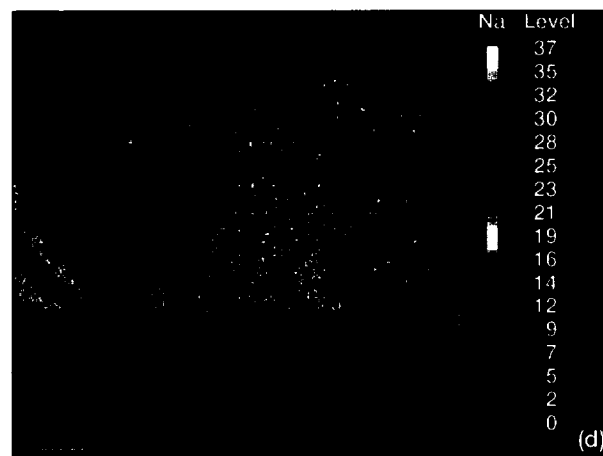
20 μm



C 20 μm

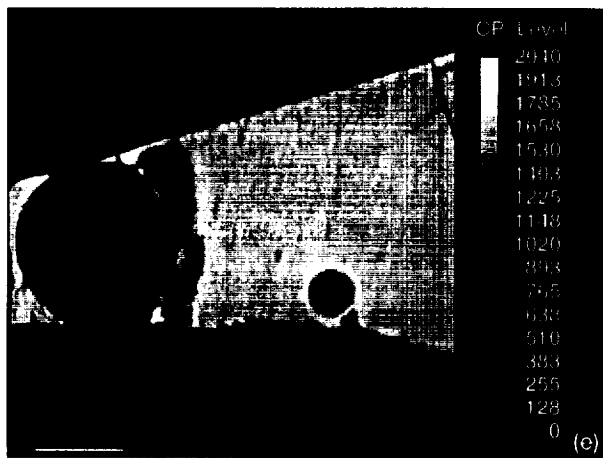


Cl 20 μm

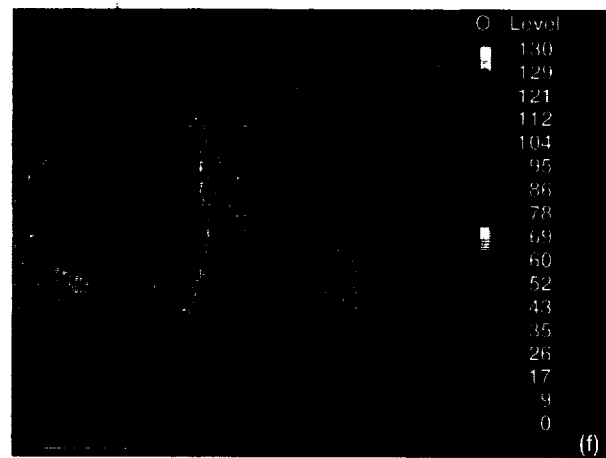


Na 20 μm

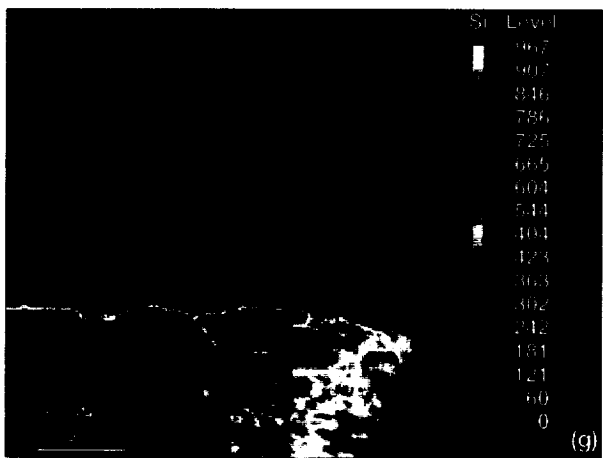
Figure 18.—Protected RCC material reacted with ZnO for 27 0.5 hr, cycles at 1200 °C in 1 atm air, region showing ZnO-Na₂O-SiO₂ glass adjacent to SiC. EPMA results—BSE image and associated elemental maps.



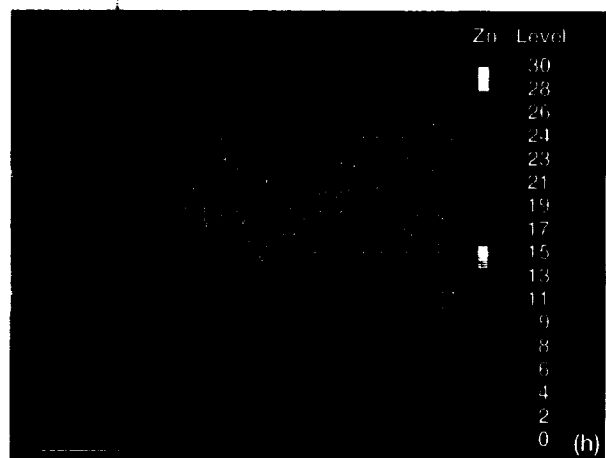
20 μm



O 20 μm



Si 20 μm



Zn 20 μm

Figure 18.—Concluded.

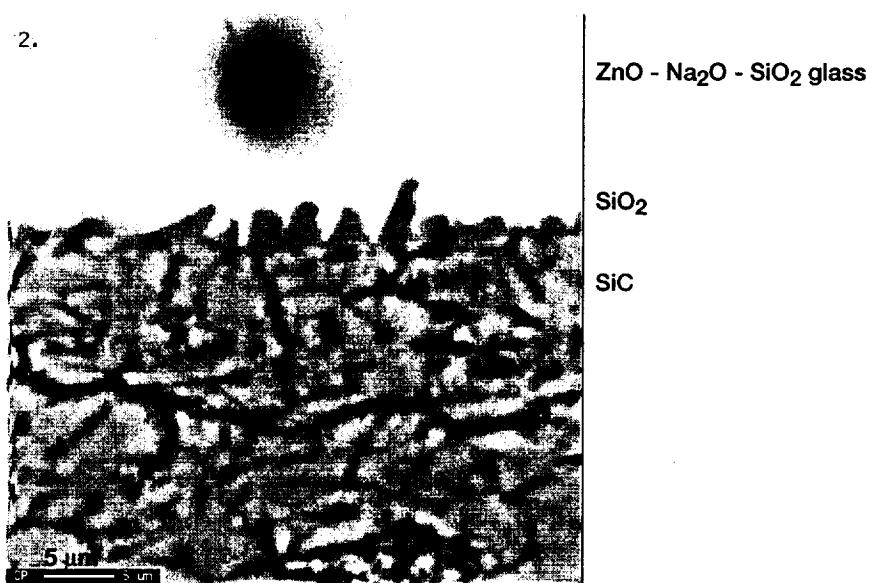


Figure 19.—Protected RCC material reacted with ZnO for 27 0.5 hr, cycles at 1200 °C in 1 atm air, region showing ZnO-Na₂O-SiO₂ glass adjacent to SiC. High magnification photograph showing glass/SiC interface—note intermediate layer of SiO₂ crystallites.

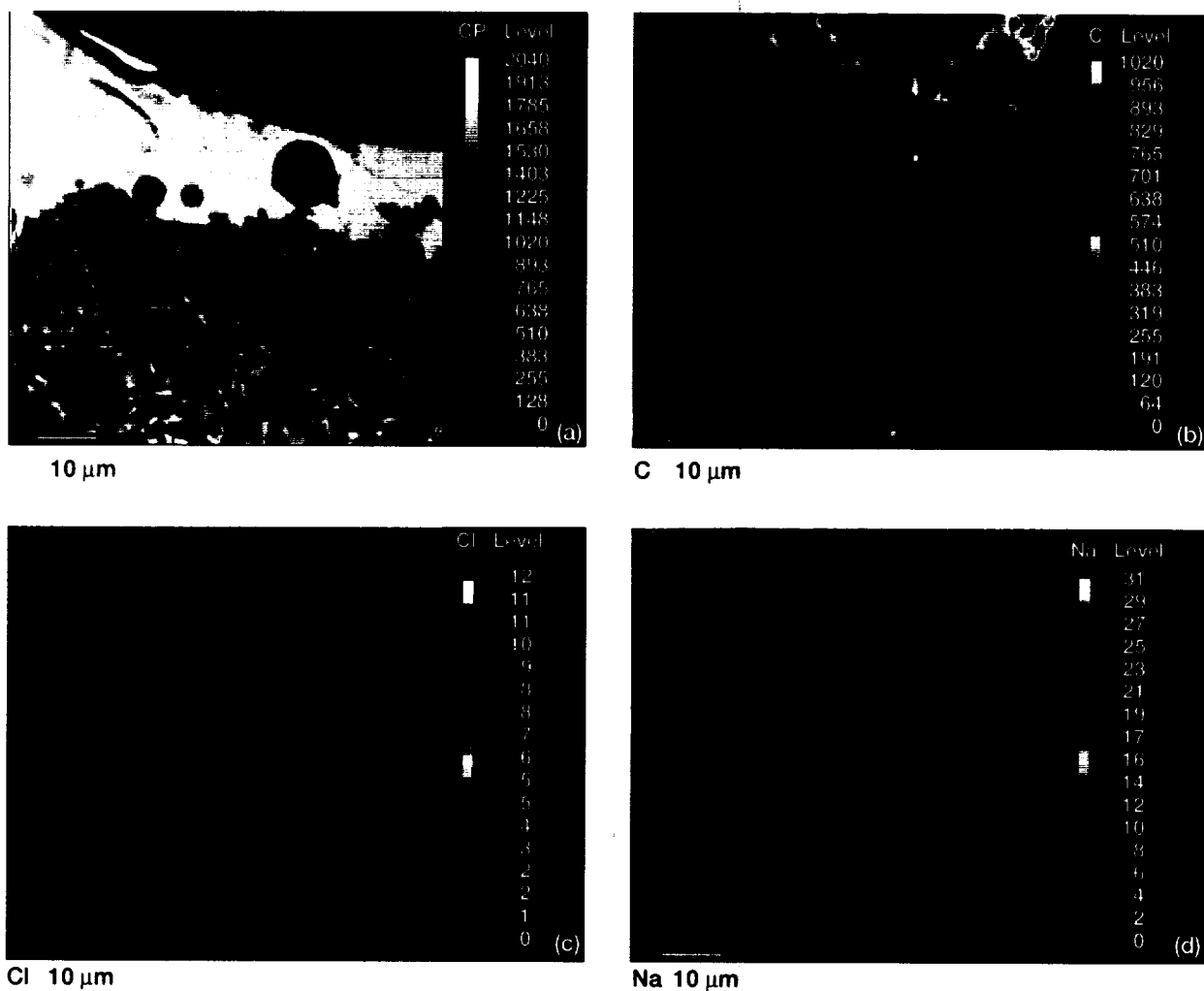


Figure 20.—Protected RCC material reacted with ZnO for 27 0.5 hr, cycles at 1200 °C in 1 atm air, region showing ZnO-Na₂O-SiO₂ glass adjacent to a portion of the SiC layer, rich in SiO₂. EPMA results—BSE image and associated elemental maps.

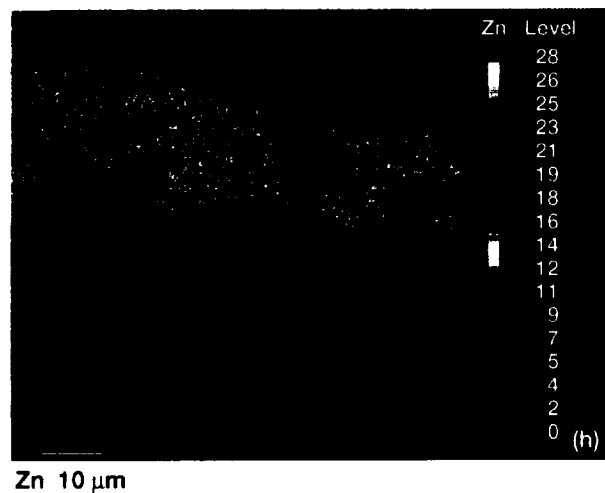
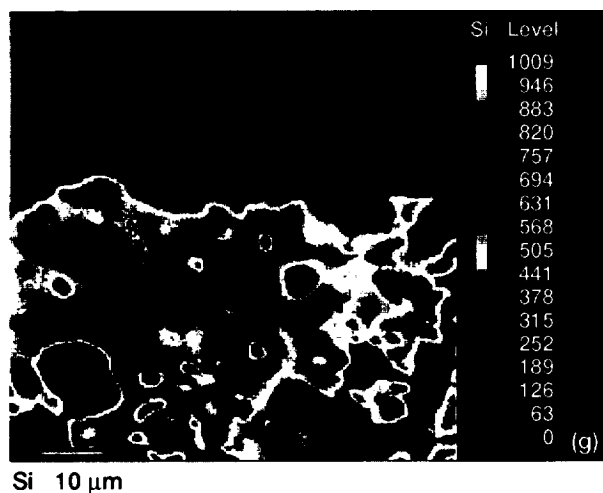
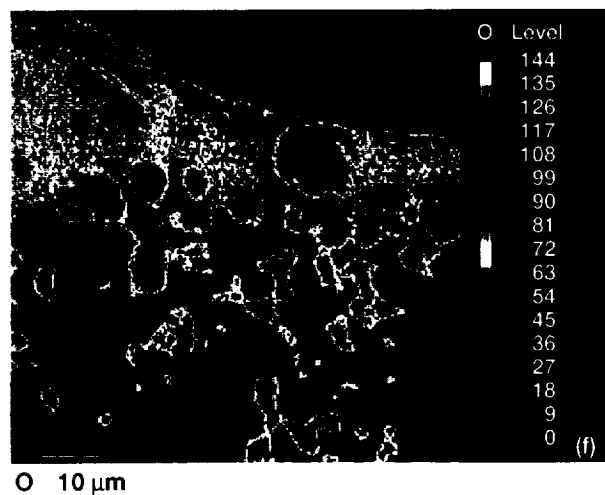
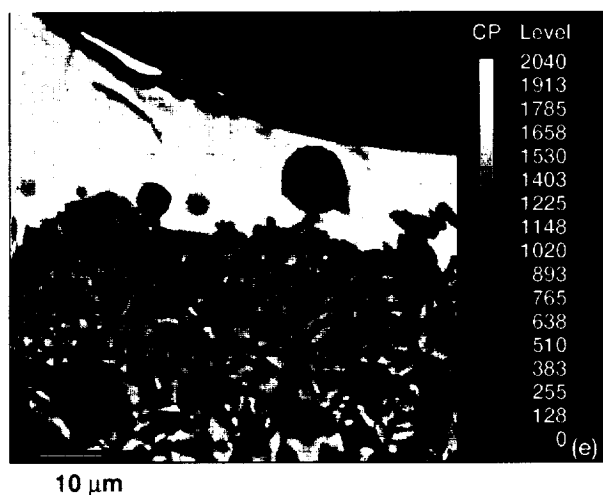
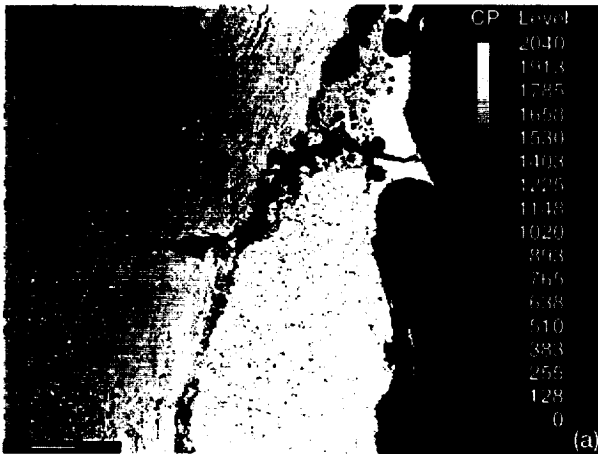
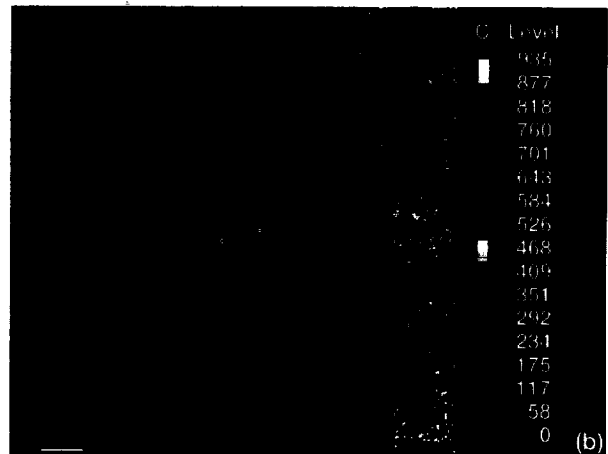


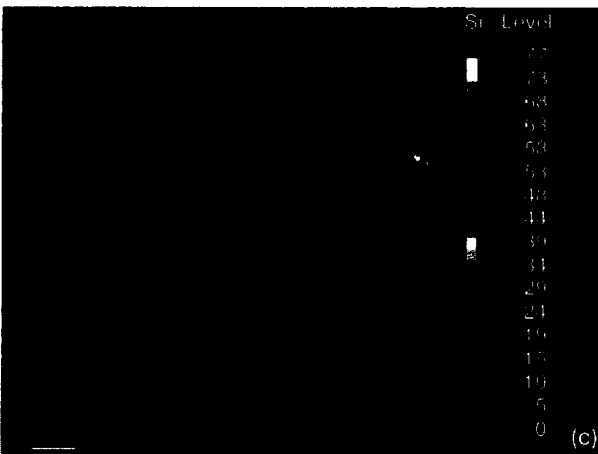
Figure 20.—Concluded.



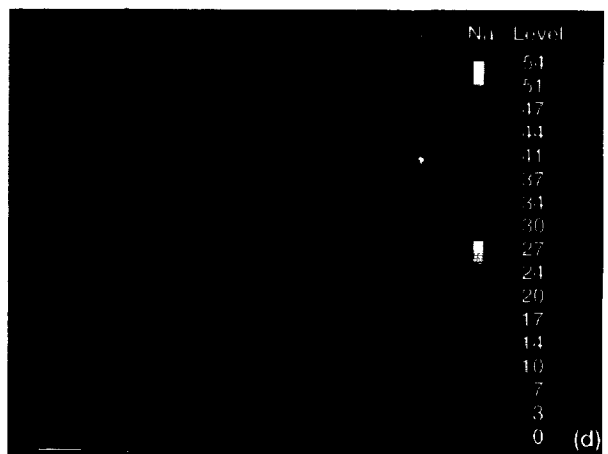
50 μm



C 50 μm



Cl 50 μm



Na 50 μm

Figure 21.—Protected RCC material reacted with ZnO for five 0.5 hr, cycles at 1200 °C in 1 atm air, region showing ZnO-Na₂O-SiO₂ glass adjacent to SiC. After the four cycles a film of NaCl was sprayed on this sample and the sample was cycled one more time. EPMA results—BSE image and associated elemental maps. Note NaCl in primarily on top but some appears to have penetrated the crack.

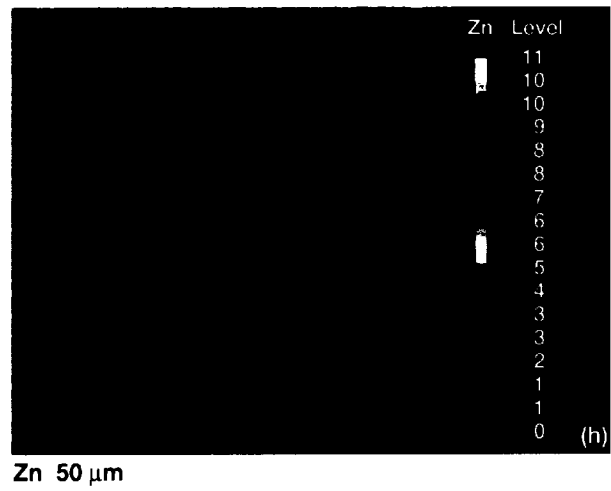
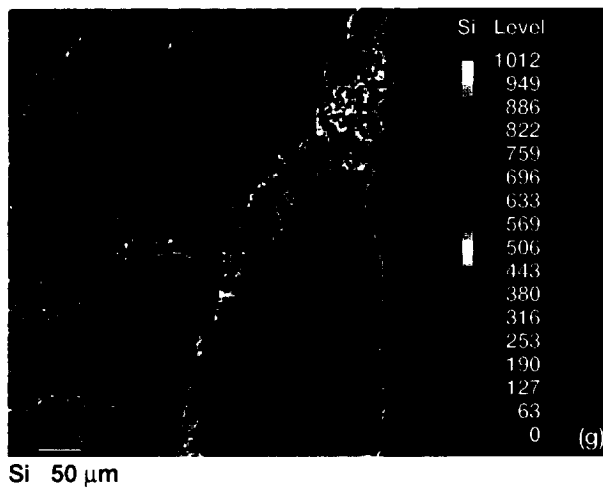
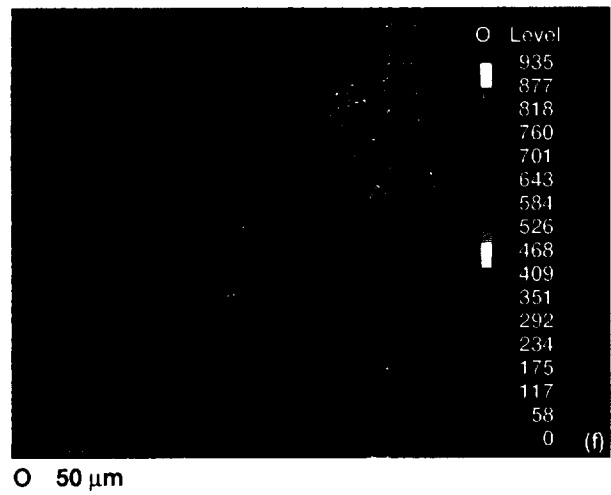
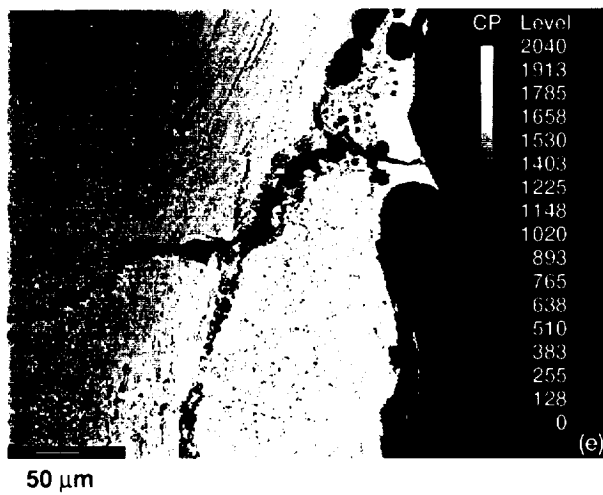


Figure 21.—Concluded.

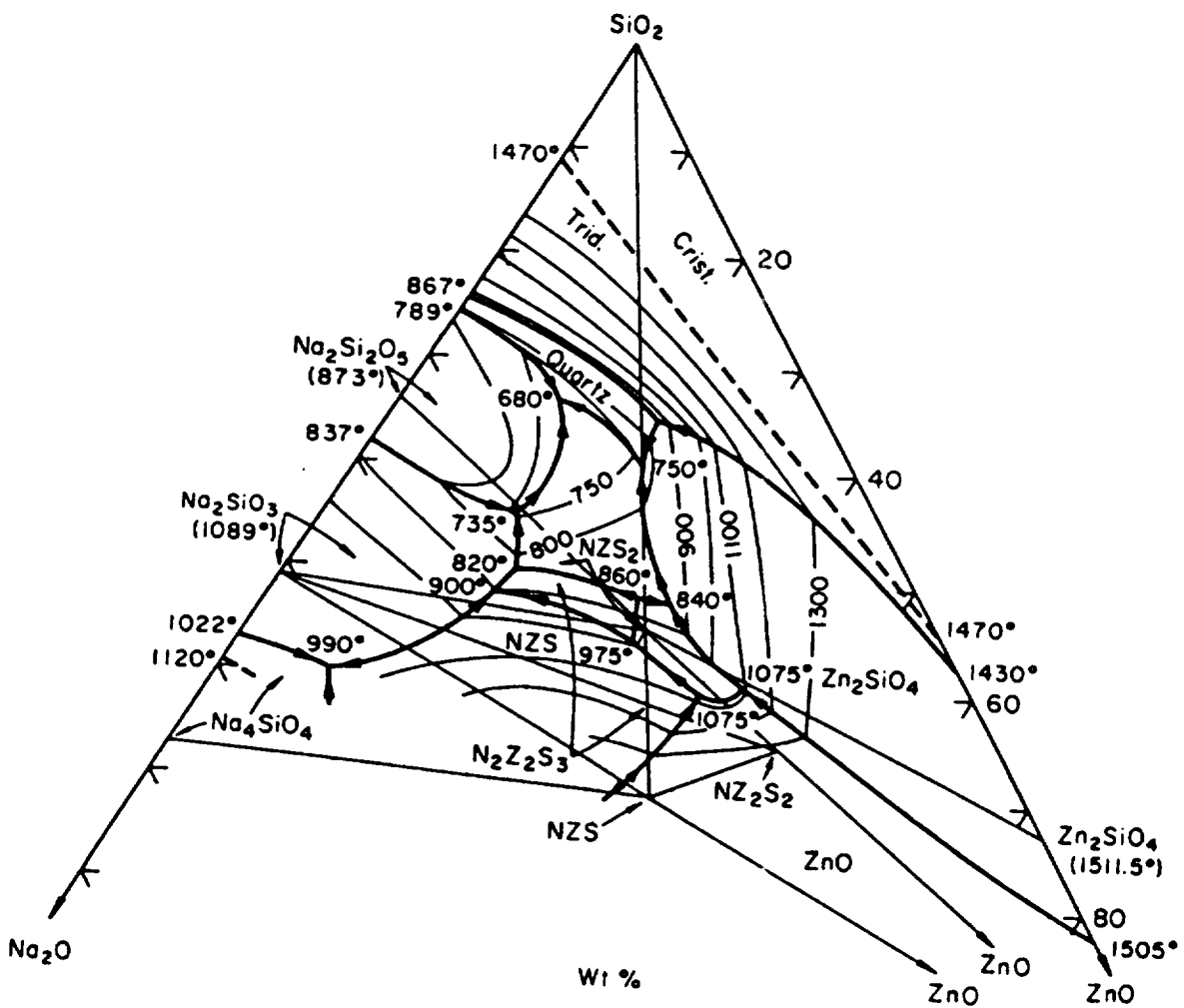
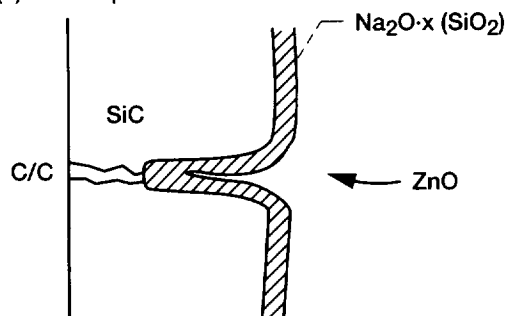
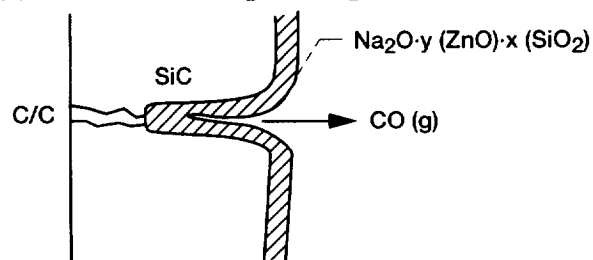


Figure 22.—ZnO-Na₂O-SiO₂ Ternary Phase Diagram (ref. 16).

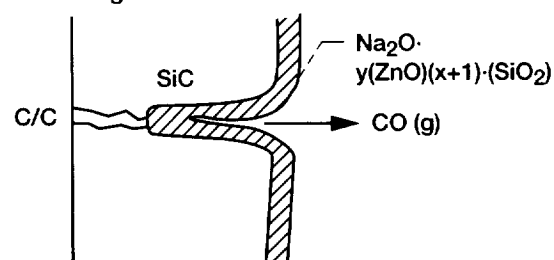
(a) ZnO deposits in crack.



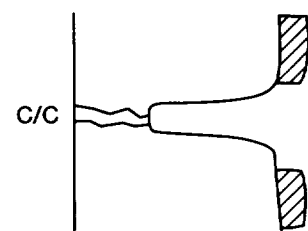
(b) ZnO reacts with $\text{Na}_2\text{O} \cdot x (\text{SiO}_2)$.



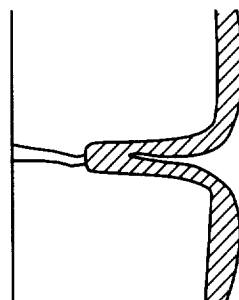
(c) $\text{Na}_2\text{O} \cdot y (\text{ZnO}) \cdot x (\text{SiO}_2)$ dissolves SiO_2 , thereby attacking SiC.



(d) SiO_2 rich $\text{Na}_2\text{O} \cdot y (\text{ZnO}) \cdot (x+1) \text{SiO}_2$ is pushed out by escaping gases, exposing fresh SiC.



(e) SiO_2 , depleted $\text{Na}_2\text{O} \cdot y (\text{ZnO}) \cdot x (\text{SiO}_2)$ flows into crack, attacking SiC.



(f) Crack is gradually enlarged. Final microstructure is shown below.

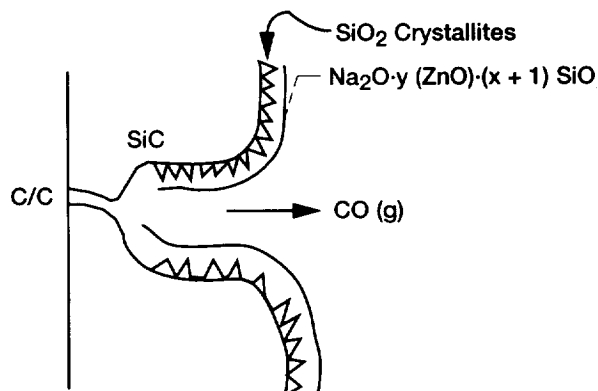


Figure 23.—Schematic of proposed pinhole formation mechanism, based on ZnO- Na_2O - SiO_2 crack enlargement. Steps (c)-(e) repeat, enlarging crack.

REPORT DOCUMENTATION PAGE			Form Approved OMB No. 0704-0188	
Public reporting burden for this collection of information is estimated to average 1 hour per response, including the time for reviewing instructions, searching existing data sources, gathering and maintaining the data needed, and completing and reviewing the collection of information. Send comments regarding this burden estimate or any other aspect of this collection of information, including suggestions for reducing this burden, to Washington Headquarters Services, Directorate for Information Operations and Reports, 1215 Jefferson Davis Highway, Suite 1204, Arlington, VA 22202-4302, and to the Office of Management and Budget, Paperwork Reduction Project (0704-0188), Washington, DC 20503.				
1. AGENCY USE ONLY (Leave blank)	2. REPORT DATE November 1998	3. REPORT TYPE AND DATES COVERED Technical Memorandum		
4. TITLE AND SUBTITLE Space Shuttle Pinhole Formation Mechanism Studies		5. FUNDING NUMBERS WU-260-10-0G-00		
6. AUTHOR(S) Nathan S. Jacobson				
7. PERFORMING ORGANIZATION NAME(S) AND ADDRESS(ES) National Aeronautics and Space Administration Lewis Research Center Cleveland, Ohio 44135-3191		8. PERFORMING ORGANIZATION REPORT NUMBER E-11351		
9. SPONSORING/MONITORING AGENCY NAME(S) AND ADDRESS(ES) National Aeronautics and Space Administration Washington, DC 20546-0001		10. SPONSORING/MONITORING AGENCY REPORT NUMBER NASA TM-1998-208659		
11. SUPPLEMENTARY NOTES Responsible person, Nathan S. Jacobson, organization code 5160, (216) 433-5498.				
12a. DISTRIBUTION/AVAILABILITY STATEMENT Unclassified - Unlimited Subject Category: 27 This publication is available from the NASA Center for AeroSpace Information, (301) 621-0390.		12b. DISTRIBUTION CODE		
13. ABSTRACT (Maximum 200 words) Pinholes have been observed to form on the wing leading edge of the space shuttle after about 10-15 flights. In this report we expand upon previous observations by Christensen (1) that these pinholes often form along cracks and are associated with a locally zinc-rich area. The zinc appears to come from weathering and peeling paint on the launch structure. Three types of experimental examinations are performed to understand this issue further: (A) Detailed microstructural examination of actual shuttle pinholes (B) Mass spectrometric studies of coupons containing actual shuttle pinholes and (C) Laboratory furnace studies of ZnO/SiC reactions and ZnO/SiC protected carbon/carbon reaction. On basis of these observations we present a detailed mechanism of pinhole formation due to formation of a corrosive ZnO-Na ₂ O-SiO ₂ ternary glass, which flows into existing cracks and enlarges them.				
14. SUBJECT TERMS Carbon/carbon; Shuttle; Corrosion		15. NUMBER OF PAGES 45		
		16. PRICE CODE A03		
17. SECURITY CLASSIFICATION OF REPORT Unclassified	18. SECURITY CLASSIFICATION OF THIS PAGE Unclassified	19. SECURITY CLASSIFICATION OF ABSTRACT Unclassified	20. LIMITATION OF ABSTRACT	